






# Auxin signaling is essential for organogenesis but not for cell survival in the liverwort *Marchantia polymorpha*

Hidemasa Suzuki <sup>1,2</sup> Hirotaka Kato <sup>1,3,4</sup> Megumi Iwano <sup>1</sup> Ryuichi Nishihama <sup>1,5,\*</sup>  
and Takayuki Kohchi <sup>1,\*</sup>

- 1 Graduate School of Biostudies, Kyoto University, Kyoto 606-8502, Japan
- 2 Graduate School of Life Sciences, Tohoku University, Sendai 980-8577, Japan
- 3 Graduate School of Science, Kobe University, Kobe 657-8501, Japan
- 4 Graduate School of Science and Engineering, Ehime University, Matsuyama 790-8577, Japan
- 5 Department of Applied Biological Science, Faculty of Science and Technology, Tokyo University of Science, Noda 278-8510, Japan

\*Author for correspondence: nishihama@rs.tus.ac.jp (R.N.), tkohchi@lif.kyoto-u.jp (T.K.)

H.S., H.K., R.N., and T.K. designed the research and wrote the paper; H.S., H.K., and M.I. performed the research and analyzed the data.

The author responsible for distribution of materials integral to the findings presented in this article in accordance with the policy described in the Instructions for Authors (<https://academic.oup.com/plcell/>) is: Takayuki Kohchi (tkohchi@lif.kyoto-u.ac.jp).

## Abstract

Auxin plays pleiotropic roles in plant development via gene regulation upon its perception by the receptors TRANSPORT INHIBITOR RESPONSE 1/AUXIN SIGNALING F-BOX (TIR1/AFBs). This auxin-regulated transcriptional control mechanism originated in the common ancestor of land plants. Although the complete loss of TIR1/AFBs causes embryonic lethality in *Arabidopsis thaliana*, it is unclear whether the requirement for TIR1-mediated auxin perception in cell viability can be generalized. The model liverwort *Marchantia polymorpha* has a minimal auxin signaling system with only a single TIR1/AFB, MpTIR1. Here we show by genetic, biochemical, and transcriptomic analyses that MpTIR1 functions as an evolutionarily conserved auxin receptor. Null mutants and conditionally knocked-out mutants of MpTIR1 were viable but incapable of forming any organs and grew as cell masses. Principal component analysis performed using transcriptomes at various developmental stages indicated that MpTIR1 is involved in the developmental transition from spores to organized thalli, during which apical notches containing stem cells are established. In MpTIR1 cells, stem cell- and differentiation-related genes were up- and downregulated, respectively. Our findings suggest that, in *M. polymorpha*, auxin signaling is dispensable for cell division but is essential for three-dimensional patterning of the plant body by establishing pluripotent stem cells for organogenesis, a derived trait of land plants.

## Introduction

The common ancestors of land plants diverged from their algal sisters approximately 450 million years ago and acquired three-dimensional (3D) bodies with parenchymal cells, which contributed to their survival in the terrestrial environment (Delwiche and Cooper, 2015). The common ancestor also established several intercellular communication mechanisms mediated by plant hormones (Bowman et al., 2019). Among these, auxin is proposed to act as a morphogen, whose

localization and gradient are critical for developmental aspects such as embryonic patterning (Liao et al., 2015; Verma et al., 2021), organ orientation (Galvan-Ampudia et al., 2020; Guan and Jiao, 2020), and gravitropism (Su et al., 2017; Herud-Sikimic et al., 2021) in plants.

The auxin signal is mainly transduced into transcriptional regulation, which is mediated by TRANSPORT INHIBITOR RESPONSE 1/AUXIN SIGNALING F-BOX (TIR1/AFB) subunits of Skp1-Cullin-F-box (SCF)-type E3 ubiquitin ligase complexes

Received June 21, 2022. Accepted December 15, 2022. Advance access publication December 19, 2022

© The Author(s) 2022. Published by Oxford University Press on behalf of American Society of Plant Biologists.

This is an Open Access article distributed under the terms of the Creative Commons Attribution-NonCommercial-NoDerivs licence (<https://creativecommons.org/licenses/by-nc-nd/4.0/>), which permits non-commercial reproduction and distribution of the work, in any medium, provided the original work is not altered or transformed in any way, and that the work is properly cited. For commercial re-use, please contact [journals.permissions@oup.com](mailto:journals.permissions@oup.com)

## IN A NUTSHELL

**Background:** Land plants alternate diploid ( $2n$ ) and haploid ( $n$ ) generations. The plant hormone auxin regulates many aspects of plant development. In flowering plants, auxin is essential for the survival of the diploid generation but is dispensable in the very short haploid generation. In contrast to flowering plants, bryophytes spend most of their life cycles as haploids.

**Question:** Is auxin signaling dispensable for haploid viability in bryophytes?

**Findings:** We addressed this question with the liverwort *Marchantia polymorpha* by knocking out the sole auxin receptor gene, *MpTIR1*. We found that the knockout mutants of *MpTIR1* were able to grow as cell clumps but were incapable of forming any organs. Gene expression profile analysis showed that stem cell genes were up-regulated in the mutants and that their developmental status was in transition from immature plants to mature plants, during which three-dimensionally organized development is initiated. We also found that expression profiles of auxin-responsive genes were correlated with this developmental transition. From these data, we conclude that auxin signaling is dispensable for cell survival but critical for organ formation in the haploid-dominant bryophyte *M. polymorpha*.

**Next steps:** In land plants, organs are formed around stem cells, but not from stem cells themselves. How is auxin signaling used differently in the microenvironment around stem cells? Alternatively, how is auxin signaling excluded from stem cells? Analyzing upstream and downstream regulation by auxin signaling should provide clues to these key questions.

as auxin receptors, AUXIN/INDOLE-3-ACETIC ACID (AUX/IAA) proteins as transcriptional repressors, and AUXIN RESPONSE FACTOR (ARF) proteins as transcription factors. In this signaling pathway, auxin facilitates the interaction between the leucine-rich-repeat (LRR) domain of TIR1/AFBs and domain II (DII) of AUX/IAAs by filling a hydrophobic cavity in the LRR domain, which in turn promotes the ubiquitination of AUX/IAAs (Gray et al., 1999, 2001; Dharmasiri et al., 2005; Kepinski and Leyser, 2005; Tan et al., 2007). In the absence of auxin, AUX/IAAs interact with ARFs and repress transcription by recruiting TOPLESS (TPL) co-repressors to the target loci of ARF (Kim et al., 1997; Ulmasov et al., 1997, 1999; Tiwari et al., 2003; Szemenyei et al., 2008). In other words, in the presence of auxin, TIR1/AFBs promote the degradation of AUX/IAAs, with their DII domain acting as a degron, which in turn enables ARFs to exert transcriptional regulation.

Comprehensive phylogenetic analyses of TIR1/AFBs, AUX/IAAs, and ARFs among land plants and green algae have shown that the auxin signaling pathway was established in the common ancestor of land plants through the acquisition of the TIR1/AFB-AUX/IAA co-receptor mechanism in order to mediate transcriptional regulation by ARFs (Bowman et al., 2017; Flores-Sandoval et al., 2018; Mutte et al., 2018). The loss of all six TIR1/AFB homologs in *Arabidopsis thaliana* led to disturbed division patterns and delayed cell divisions, which led to the inhibition of embryogenesis (Prigge et al., 2020). By contrast, TIR1/AFBs do not seem to be essential in gametes, as shown by the survival of *tir1/afb* sextuple mutants, although it is possible that the gametes contain adequate levels of parental gene products to sustain auxin signaling given the short gametophytic generation time of *A. thaliana* (Prigge et al., 2020).

The moss *Physcomitrium* (*Physcomitrella*) *patens* and the liverwort *Marchantia polymorpha* have been studied as

models for gametophyte-dominant species (Rensing et al., 2020; Kohchi et al., 2021). The *P. patens* TIR1/AFB and AUX/IAA homologs undergo auxin-dependent interaction (Prigge et al., 2010). Disturbed auxin perception suppresses the differentiation of caulonema in *P. patens* (Prigge et al., 2010), whereas in *M. polymorpha*, it leads to the formation of undifferentiated cell masses (Kato et al., 2015). In these studies, auxin perception was inhibited either by knockdown of TIR1/AFBs (Prigge et al., 2010) or by the expression of non-degradable AUX/IAAs with mutations in DII (Prigge et al., 2010; Kato et al., 2015), where leaky signal transduction cannot be avoided. For this reason, it is difficult to assess the role of auxin in terms of gametophytic cell survival through the studies described above. Instead, knocking out the TIR1/AFBs is expected to shut down auxin signaling altogether. We chose *M. polymorpha* for our study, as it encodes a minimal set of auxin signaling components, including the sole TIR1/AFB and AUX/IAA homologs *MpTIR1* and *MpIAA*, respectively (Flores-Sandoval et al., 2015; Kato et al., 2015; Bowman et al., 2017).

In *M. polymorpha*, as in vascular plants, the natural auxin indole-3-acetic acid (IAA) is biosynthesized from tryptophan in a two-step reaction, which is initially catalyzed by TRYPTOPHAN AMINOTRANSFERASE OF ARABIDOPSIS (TAA) and subsequently by YUCCA (YUC) homologs (Eklund et al., 2015). Knockout (KO) of the sole TAA gene, *MpTAA*, generates cell masses with no obvious organogenesis. However, it is unclear whether these developmental defects are due to the loss of auxin signaling or the loss of other functions of the biosynthesized auxin.

Germinated *M. polymorpha* spores divide vigorously to produce unorganized tissues known as sporelings. Once single-celled apical stem cells are established, they initiate 3D morphogenesis into thalli, on which specialized organs

such as the gemma cups are differentiated (Shimamura 2016; Kohchi et al., 2021). Within the dorsal organ gemma cup, multicellular asexual reproductive propagules known as gemmae are produced from single initial cells, which involves apical stem cell formation (Kato et al., 2020b). Auxin acts as a mobile signal in the thalli (Gaal et al., 1982; Solly et al., 2017), and auxin signaling regulates the establishment of the body axis during gemma development (Kato et al., 2017, 2018). Here, to explore the requirement for and roles of auxin signaling in plant development, we analyzed the molecular functions of MpTIR1 as an auxin receptor and performed a knockout study of MpTIR1 in the liverwort *M. polymorpha*. Our findings uncover the requirement for auxin signaling in organogenesis but not cell survival in *M. polymorpha*.

## Results

### MpTIR1 positively regulates auxin responses

To determine whether MpTIR1 is involved in auxin responses, we exogenously treated wild-type (WT) plants, MpTIR1-overexpressing plants as well as *Mptir1* mutants with varying concentrations of natural (indole-3-acetic acid (IAA)) and synthetic (1-naphthaleneacetic acid (NAA) and 2,4-dichlorophenoxyacetic acid (2,4-D)) auxins. For overexpression, MpTIR1 was driven by the *MpEF1A* promoter (Figure 1A), which confers strong and ubiquitous transgene expression (Althoff et al., 2014). WT plants showed ectopic rhizoid formation and arrested thallus development in the presence of high levels of auxin (Figure 1, B and C; Supplemental Figure 1, A–D). Consistent with the assumption that MpTIR1 is an auxin receptor, MpTIR1-overexpressing plants exhibited hypersensitivity to auxins; the responses were observed at lower auxin concentrations (Figure 1, B and C; Supplemental Figure 1).

*Mptir1-1<sup>ko</sup>* mutants grew as cell masses with no obvious organ development (Supplemental Figure 2; see “MpTIR1 is critical for organ development but dispensable for cell survival” for details); exogenous auxins neither caused morphological changes nor enhanced rhizoid development in *Mptir1-1<sup>ko</sup>* cells, although NAA and 2,4-D, but not IAA, slightly affected the increase in growth (Figure 1D; Supplemental Figure 2, D and E). *Mptir1-1<sup>ko</sup>* mutants harboring a transgene of a MpTIR1 genomic fragment showed rescued morphology with normal auxin responsiveness, as shown by ectopic rhizoid formation and arrested growth in the presence of high concentrations of auxin (Figure 1D). This was also the case with *Mptir1-1<sup>ko</sup>* mutants harboring the *A. thaliana* TIR1 (*AtTIR1*) transgene driven by the MpTIR1 promoter (Figure 1D). These results suggest that MpTIR1 positively regulates auxin responses and that its function is comparable with that of *AtTIR1*.

### MpTIR1 acts as an auxin receptor

Interactions between TIR1/AFBs and AUX/IAAs and the subsequent degradation of AUX/IAAs are essential for auxin

signaling (Gray et al., 1999; 2001; Dharmasiri et al., 2005; Kepinski and Leyser, 2005). To investigate whether MpTIR1 requires auxin for its interaction with MplAA, we performed an in vitro pull-down assay. We used the *Escherichia coli*-expressed fusion protein of glutathione S-transferase (GST) with MplAA truncated from the 627th amino acid to the C-terminus including DII (GST-MplAA(627C)) as the bait for *M. polymorpha*-expressed MpTIR1-3xFLAG. The MpTIR1-3xFLAG proteins showed interactions with MplAA only when auxin was added to the mixture (Figure 2A). IAA facilitated the MpTIR1-MplAA interaction in a dose-dependent manner (Figure 2A). NAA and 2,4-D also mediated the MpTIR1-MplAA interaction as IAA (Figure 2A). GST-MplAA<sup>mutDII</sup>(627C), which harbors a mutated sequence in its DII that had been shown to inhibit auxin signaling in *M. polymorpha* (Kato et al., 2015), did not interact with MpTIR1 regardless of the presence of auxin (Figure 2B). These data suggest that MpTIR1 interacts with the DII of MplAA in an auxin-dependent manner.

We also investigated the involvement of MpTIR1 in the degradation of MplAA in vivo using conditional knockout (CKO) mutants generated by transforming *Mptir1-1<sup>ko</sup>* cells with a vector (Nishihama et al., 2016) that, under normal conditions, expressed a floxed (flanked by loxP) MpTIR1 coding region driven by the *MpEF1A* promoter for complementation. After induction by heat shock and dexamethasone (DEX) treatment, Cre recombinase excised the floxed MpTIR1 to express nuclear localization signal (NLS)-fused Citrine for labeling MpTIR1-KO cells (Supplemental Figure 3, A–C). Hereafter, we refer to these plants as *Mptir1-1<sup>CKO > CitN</sup>* plants. We then assessed the accumulation of a DII degenon peptide probed by mTurquoise2-NLS in *Mptir1-1<sup>CKO > CitN</sup>* plants. If MpTIR1 targets MplAA for degradation by recognizing the DII degenon, accumulation of DII-mTurquoise2-NLS would be facilitated in the absence of MpTIR1. Stronger mTurquoise2-fluorescence signals were detected under MpTIR1 KO-induced conditions than uninduced conditions (Figure 2, C and D). By contrast, the mutated DII peptide (see above) failed to enhance mTurquoise2 fluorescence signals under MpTIR1 KO-induced conditions (Figure 2, C and D). These results suggest that MpTIR1 promotes the degradation of MplAA in a DII-dependent manner in vivo, which is a direct indication that MpTIR1 acts as an auxin receptor.

### MpTIR1 is essential for auxin-mediated transcriptional regulation

In order to analyze MpTIR1-mediated auxin-dependent transcriptional regulation, WT (5-day-old sporelings) and *Mptir1-1<sup>ko</sup>* cells were treated with or without 10  $\mu$ M IAA as well as 10  $\mu$ M NAA for 4 h and then subjected to RNA-seq analyses to compare their transcriptome profiles. Differentially expressed genes (DEGs) were examined compared to mock-treated (without auxin) samples for each experiment (Supplemental Data Set 1).

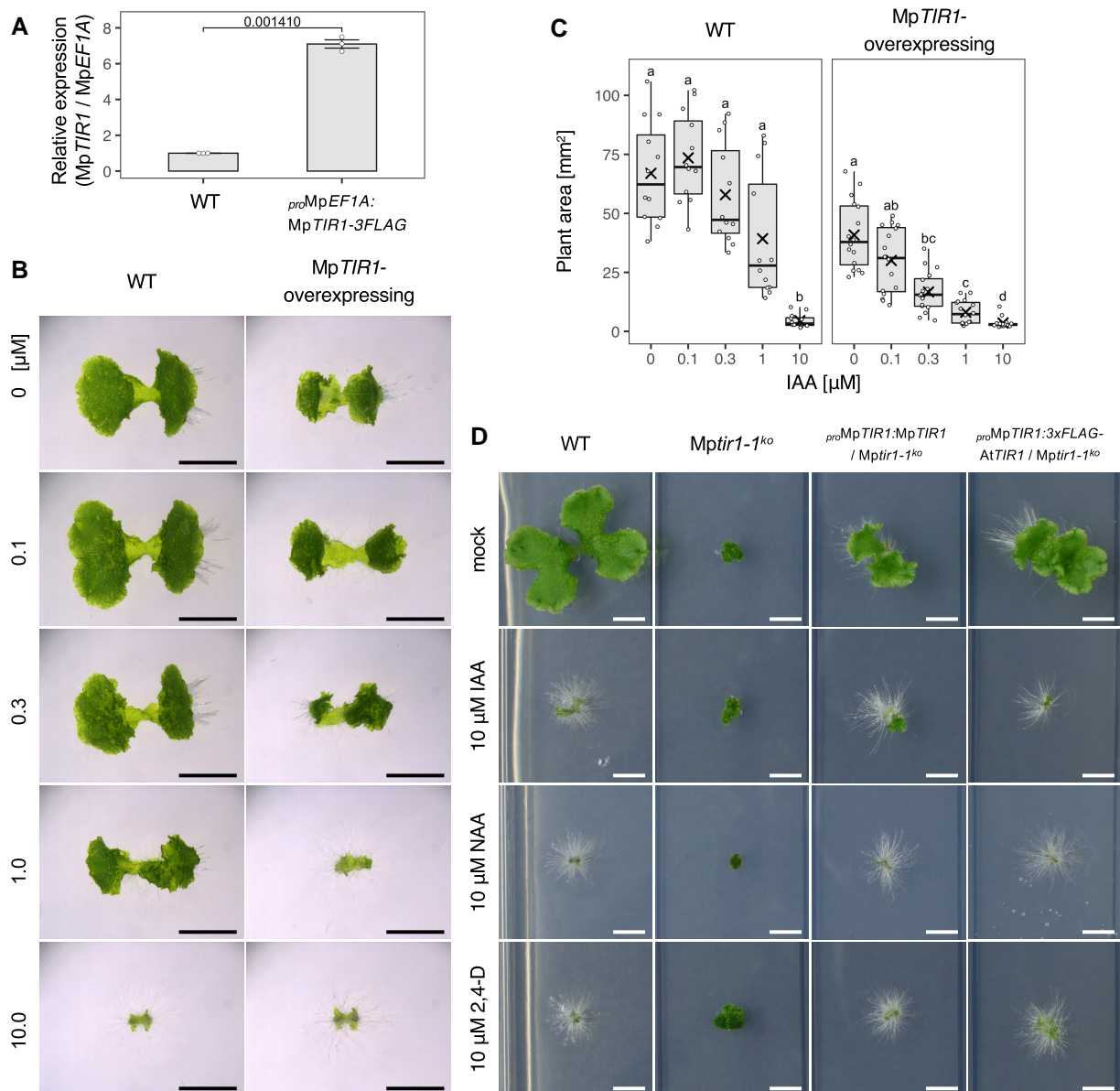


**Figure 1** Genetic evidence for *MpTIR1* as an auxin receptor-encoding gene. **A**, Relative expression levels of *MpTIR1* in *MpTIR1*-overexpressing plants to wild type (WT). RT-qPCR was performed in 10-day-old thalli. Cq values of *MpTIR1* were normalized to those of *MpEF1A*. Dots indicate each value from three biological replicates. Error bars indicate mean  $\pm$  standard error ( $\sigma$ ). The value above the plots indicates the *P*-value of two-sided Welch's *t*-test. **B** and **C**, Responsiveness of WT and *MpTIR1*-overexpressing plants to exogenously supplied auxin. Gemmae were grown on agar medium containing the indicated concentrations of IAA for 10 days. **B**, A representative image is shown for each condition. Scale bars = 5 mm. **C**, Boxplot of thallus areas. The bands and crosses inside the boxes represent median and mean, respectively. The lower and upper hinges correspond to the first and third quartiles, respectively. Whiskers extend from the hinges to the smallest and largest values no further than  $1.5 \times$  IQR from the hinge (where IQR is the inter-quartile range). Dots represent each value of  $\geq 12$  independent plants. Significance was tested by Steel–Dwass test with 99% significance level. **D**, Responsiveness of WT, *Mptir1-1<sup>ko</sup>* mutants, *proMpTIR1: MpTIR1 / Mptir1-1<sup>ko</sup>* plants, and *proMpTIR1:3xFLAG-AtTIR1 / Mptir1-1<sup>ko</sup>* plants to auxin. Small clumps of cell masses (of *Mptir1-1<sup>ko</sup>*) or gemmae (of the others) were grown for 14 days in the absence or presence of 10  $\mu$ M each of IAA, NAA, or 2,4-D. Scale bars = 5 mm.

In the WT samples, IAA treatment caused the up- and down-regulation of 83 and 76 genes, respectively ( $p_{adj} < 0.001$ ) (Figure 3A). NAA treatment yielded  $>15$ -fold larger numbers of DEGs than did IAA treatment (Figure 3A). Nevertheless, the majority of DEGs under IAA treatment were also differentially expressed in response to NAA with a high correlation

(Supplemental Figure 4, A and B). These results suggest that although NAA acts more strongly than IAA, both auxins essentially induce the same transcriptional changes.

In a previous study, RNA-seq of thalli treated with or without 2,4-D for 1 h was reported (Mutte et al., 2018). We re-analyzed the data with our pipeline and found 57

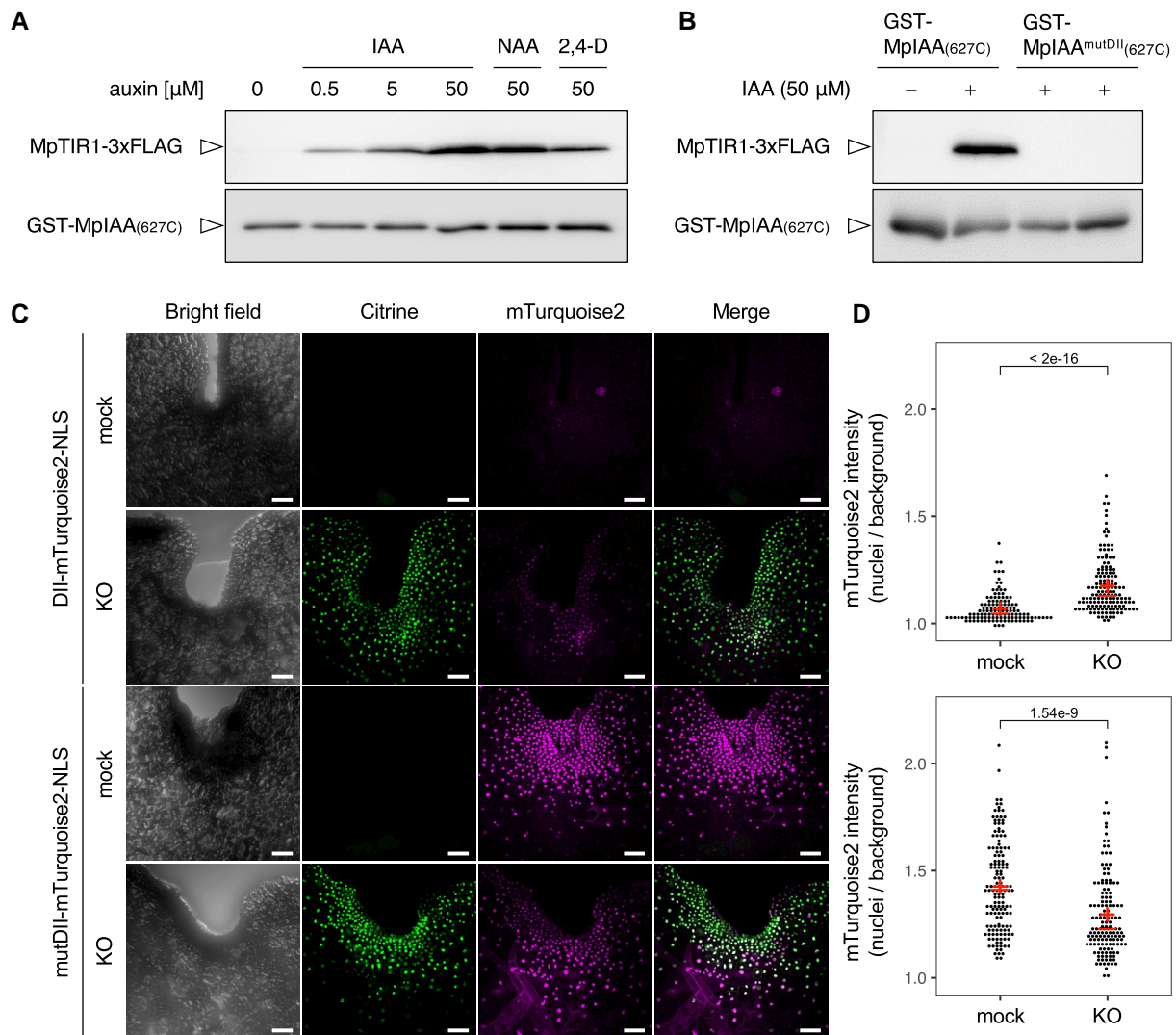


**Figure 2** Molecular evidence for MpTIR1 as an auxin receptor. A and B, Pull-down assay between MpIAA and MpTIR1. Bead-bound GST-MpIAA(627C) protein, which had been expressed in and purified from *E. coli*, was incubated with a protein extract from MpTIR1-3xFLAG-expressing *M. polymorpha* plants in the presence or absence of the indicated concentrations of IAA, 50  $\mu$ M NAA, or 50  $\mu$ M 2,4-D. Bead-bound proteins were washed and subjected to immunoblot analysis with anti-FLAG (top) or anti-GST (bottom) antibody. B, Pull-down assay using a DII-mutated MpIAA. GST-MpIAA(627C) or GST-MpIAA<sup>mutDII</sup>(627C), with a mutation in DII, were incubated with a protein extract from MpTIR1-3xFLAG-expressing *M. polymorpha* plants in the presence or absence 50  $\mu$ M IAA. C, Stabilization of the DII of MpIAA after conditional KO of MpTIR1. One-day-old gemmalings of *pro*MpEF1A:DII-mTurquoise2-NLS/Mptir1-1<sup>CKO > CitN</sup> (top) or *pro*MpEF1A:mutDII-mTurquoise2-NLS/Mptir1-1<sup>CKO > CitN</sup> (bottom) were either mock-treated or dexamethasone-treated (KO), subjected to heat shock, and further grown for 1 d. Bright field, Citrine fluorescence, mTurquoise2 fluorescence, and their merged images of a notch region are shown. Scale bars = 50  $\mu$ m. D, Quantification of mTurquoise2 fluorescence intensities in individual nuclei in the experiments shown in (C). Dot plots of *pro*MpEF1A:DII-mTurquoise2-NLS/Mptir1-1<sup>CKO > CitN</sup> (top) or *pro*MpEF1A:mutDII-mTurquoise2-NLS/Mptir1-1<sup>CKO > CitN</sup> (bottom) are shown. The values above the plots indicate *P*-values of Brunner–Munzel test between the mock conditions and KO-induced conditions. The red crosses and bars indicate means and medians, respectively. *n* = 125 or 150 nuclei from 5 or 6 different plants.

upregulated genes and 53 downregulated genes ( $p_{adj} < 0.01$ ), among which 35 and 28 genes had  $p_{adj} < 0.001$ , respectively (Supplemental Data Set 2). The transcription factor genes MpC2HDZ, MpWIP, MpLRL, and MpR2R3-MYB21 were upregulated under all conditions, regardless of the differences in auxin type, treatment duration, or state of plant differentiation (Supplemental Figures 5–7). By contrast, the auxin biosynthetic enzyme genes MpTAA and MpYUC2 were downregulated

under all conditions. These factors may be central regulatory targets of auxin signaling in *M. polymorpha*.

In *Mptir1-1<sup>ko</sup>* cells, consistent with MpTIR1 being an auxin receptor, almost no DEGs were detected upon IAA treatment (1 gene upregulated, 0 genes downregulated at  $p_{adj} < 0.001$ ; Figure 3A). Dramatically fewer DEGs were also detected upon NAA treatment (112 upregulated genes and 253 downregulated genes at  $p_{adj} < 0.001$ ) compared to the

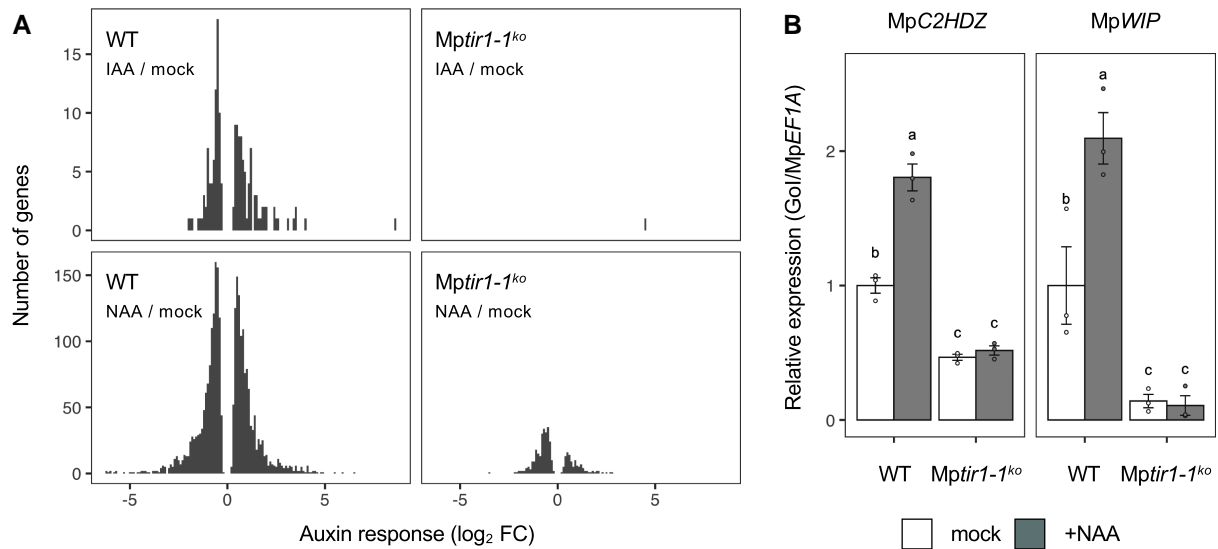


**Figure 3** Nearly absolute requirement for MpTIR1 in transcriptional responses to auxin. A, RNA-seq analysis of *Mptir1-1<sup>ko</sup>* cells. x- and y-axes represent log<sub>2</sub> fold changes (log<sub>2</sub> FC) and numbers of differentially expressed genes ( $p_{adj} < 0.001$ ) in response to IAA (top) or NAA (bottom) treatment in WT sporelings (left) and *Mptir1-1<sup>ko</sup>* cells (right). Note that the y-axis value of NAA-responsive genes is 10-fold larger than that of IAA. B, Relative expression levels of known auxin-responsive genes, *MpC2HDZ* and *MpWIP*, determined by RT-qPCR. Five-day-old sporelings and *Mptir1-1<sup>ko</sup>* cells were treated with 10  $\mu$ M of NAA or solvent control (mock) for 4 h. *MpEF1A* was used for normalization. Expression levels relative to mock-treated WT sporelings were plotted. Dots indicate each value from three independent plants. Error bars indicate mean  $\pm$  SE. Significance was tested by one-way ANOVA followed by Tukey–Kramer test with 99.9% significance level.

WT (Figure 3A). The hypo- or non-responsiveness of *Mptir1-1<sup>ko</sup>* cells to auxin was further confirmed by reverse transcription quantitative PCR (RT-qPCR) on known auxin-responsive genes, *MpC2HDZ* and *MpWIP* (Figure 3B; Kato et al., 2017, 2020a; Mutte et al., 2018). These results further confirm the role of MpTIR1 in auxin-mediated transcriptional regulation. Nevertheless, NAA still caused transcriptional changes in *Mptir1-1<sup>ko</sup>* cells (Figure 3A; Supplemental Data Set 3). Gene ontology (GO) term enrichment analysis of these DEGs showed that genes related to some specific processes, such as protein folding, were upregulated, while genes related to metabolic processes were downregulated (Supplemental Figure 8; Supplemental Data Sets 4 and 5). These results suggest that NAA also induces MpTIR1-independent responses, although whether this reflects the action of NAA as a phytohormone is unclear.

### MpTIR1 is critical for organ development but dispensable for cell survival

To explore the role of TIR1-mediated auxin signaling in 3D morphogenesis, we knocked-out MpTIR1 using homologous recombination-mediated gene targeting in WT sporelings. The resulting five independent *Mptir1-1<sup>ko</sup>* mutants failed to develop thalli and slowly proliferated as cell masses (Figure 4A; Supplemental Figures 2, A and B and 9). We did not observe any phenotypic differences between male and female mutants (Supplemental Figure 2C). The mutants displayed disordered cell division in the cell masses and failed to differentiate into multicellular organs and rhizoids (Figure 4B). We generated additional mutants with deletions of the entire MpTIR1 genomic

locus using CRISPR/Cas9 genome editing (Supplemental Figure 10). All four independent deletion mutants (*Mptir1-2<sup>ld</sup>*, *Mptir1-3<sup>ld</sup>*, *Mptir1-4<sup>ld</sup>*, and *Mptir1-5<sup>ld</sup>*) displayed similar phenotypes to those of the *Mptir1-1<sup>ko</sup>* mutants (Supplemental Figure 11). The developmental defects of the *Mptir1-1<sup>ko</sup>* mutants, besides the auxin response defects described above, were rescued by the introduction of MpTIR1 or AtTIR1 transgenes driven by the MpTIR1 promoter (Figure 1D), confirming that the impaired organogenesis of *Mptir1-1<sup>ko</sup>* mutants was due to the loss of evolutionarily conserved functions of MpTIR1. For a more detailed understanding, we compared the cell compositions of *Mptir1-1<sup>ko</sup>* cell clumps with that of proliferating WT sporelings. Ten-day-old sporelings contained meristematic region(s) consisting of small undifferentiated cells and other regions containing large vacuolated cells (Figure 4, C and D). *Mptir1-1<sup>ko</sup>* cell masses were not composed of a uniform cell type but a mixture of small cells at the outer regions and large vacuolated cells at the inner regions (Figure 4, E and F). Taken together, these results suggest that MpTIR1 is dispensable for cell survival but is essential for orderly organogenesis and development.

### MpTIR1 is critical for proper patterning and organ differentiation

In order to determine the physiological roles of MpTIR1 in other developmental stages, we generated *Mptir1-1<sup>CKO</sup> > CitN* plants (see “MpTIR1 acts as an auxin receptor” section) and *Mptir1-1<sup>CKO</sup> > tdTN* plants. In the latter plants, *Mptir1-1<sup>ko</sup>* cells could be visualized using tdTomato-NLS after excision of the floxed MpTIR1 genomic fragment (Figure 5A; Sugano et al.,

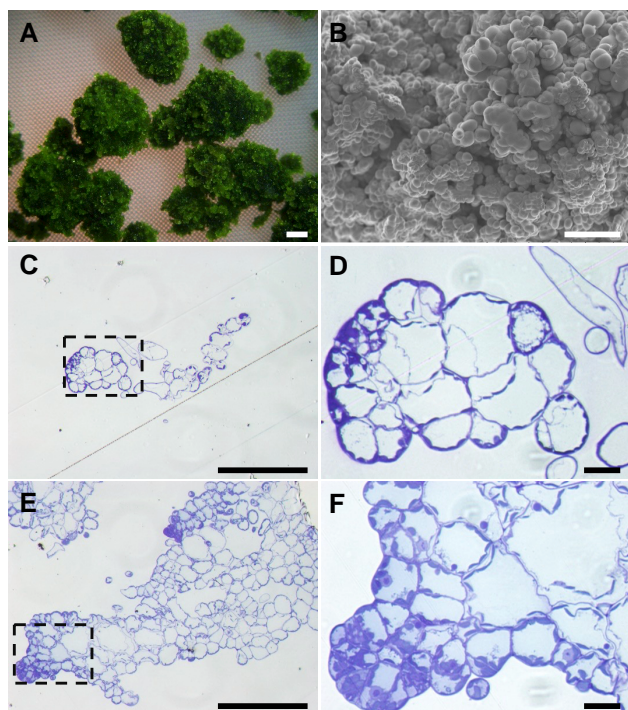


**Figure 4** Requirement for MpTIR1 in organogenesis. A, *Mptir1-1<sup>ko</sup>* cell masses. *Mptir1-1<sup>ko</sup>* cells were grown on agar medium for 56 days. Images of whole plates are shown in Supplemental Figure 9. B, A SEM image of *Mptir1-1<sup>ko</sup>* cell masses. A clump of 90-day-old *Mptir1-1<sup>ko</sup>* cells was observed. C–F, Sections of WT sporelings (C, D) and *Mptir1-1<sup>ko</sup>* cell masses (E, F). D and F, Magnified images of the areas within the dashed lines in (C) and (E), respectively. Scale bars = 1 mm (A), 200  $\mu$ m (B, C, E), 20  $\mu$ m (D, F).

2018; Suzuki et al., 2020). *Mptir1<sup>CKO</sup> > tdTN* gemmae essentially showed proper patterning with a trace of stalk at the bottom and two apical notches at its lateral tips (Figure 5B). When we excised the floxed MpTIR1 transgene during gemma development, the gemma patterning appeared disordered and failed to establish ellipse-shaped bodies and notches (Figure 5C). We then examined the phenotypes resulting from the loss of MpTIR1 after the germination of gemmae. *Mptir1-1<sup>CKO</sup> > CitN* and *Mptir1-1<sup>CKO</sup> > tdTN* gemmae grew into thalli under mock conditions, whereas the excision of the floxed MpTIR1 transgene in mature gemmae or 1-day-old gemmalings resulted in impaired thallus development and caused cell mass formation (Figure 5, D–H; Supplemental Figure 3, B and C). These results suggest that MpTIR1 is critical for proper patterning and organ differentiation in *M. polymorpha*.

### Auxin hypo-responsiveness is a common feature of *Mptir1-1<sup>ko</sup>* cells and sporelings

In order to clarify the properties of *Mptir1-1<sup>ko</sup>* cells, we assessed the gene expression patterns using principal component analysis (PCA) of *Mptir1-1<sup>ko</sup>* cells, sporelings, and available organ-specific transcriptome data (Frank and Scanlon, 2015; Higo et al., 2016; Bowman et al., 2017; Yasui et al., 2019). In the two-dimensional plot of the first and second principal components

(PC1 and PC2, respectively), biological replicates from the same sources were clustered (Figure 6A). WT tissues were grouped into an approximate order of developmental stage (Figure 6A). Spores and sporelings were grouped age-wise along PC2, and these developmentally early tissues were grouped separately from the thalli, reproductive organs, and sporophytes along PC1 (Figure 6A). Vegetative thalli and gemma cups were comparable to older sporelings in PC2, while reproductive organs and sporophytes were grouped along PC2 (Figure 6A). Interestingly, *Mptir1-1<sup>ko</sup>* cells were grouped within a similar PC2 score range on the developmental trajectory from spores/sporelings to thalli (Figure 6A).

To explore the relationships between the developmental trajectory and auxin responsiveness, we performed another PCA using a subset that included *Mptir1-1<sup>ko</sup>* cells, 5-day-old sporelings, and thalli (Figure 6B). PC1 scores were high in *Mptir1-1<sup>ko</sup>* and sporelings, but low in thalli, resulting in a large separation along PC1 (Figure 6B). In order to determine whether auxin responsiveness contributed to this particular separation, we examined its relationships to factor loadings for PC1 and PC2. Genes that were downregulated upon IAA treatment were dense in positive factor loading of PC1, whereas upregulated genes were dense in the negative factor loading of the PC1 (Figure 6C). These relationships suggest that IAA-responsive gene expression patterns contributed to the PC1 values. By contrast, we did not find any correlation between IAA responsiveness and factor loading of the PC2 (Figure 6D). Similar relationships were observed with respect to NAA treatment (Supplemental Figure 12, A and B). These observations suggest that auxin hypo-responsiveness is a characteristic feature of sporelings and that *Mptir1-1<sup>ko</sup>* mutants failed to differentiate from sporelings to thalli due to defects in their auxin response.

In order to understand what causes the auxin hypo-responsiveness of sporelings, we examined the expression patterns of auxin biosynthesis and signaling genes with RNA-seq data (Supplemental Figure 13, A and B). MpTIR1 transcripts were abundantly detected in both sporelings and thalli (Supplemental Figure 13C). In fact, the MpTIR1 promoter-driven MpTIR1-tdTomato fusion protein, which complemented the *Mptir1-1<sup>ko</sup>* mutants, accumulated at nucleus-like regions in most of the sporeling cells soon after germination (Supplemental Figure 14). Meanwhile, the transcript levels of MpYUC2, a major vegetative YUC homolog, and some other auxin signaling components (i.e. MpIAA, MpARF1, MpARF2, and MpNONCANONICAL ARF [MpNCARF]) were lower in sporelings than in thalli (Supplemental Figure 13C). These results suggest that sporeling hypo-responsiveness is not due to a lower capacity for auxin perception but is due to low auxin production and/or less dynamic transcription of downstream genes.

### MpTIR1 promotes gene expression for organ differentiation

To further characterize the differentiation features of *Mptir1-1<sup>ko</sup>* cells, we performed transcriptomic pairwise comparisons of *Mptir1-1<sup>ko</sup>* cells with sporelings and thalli (Supplemental Data Set 6). With respect to regulatory genes

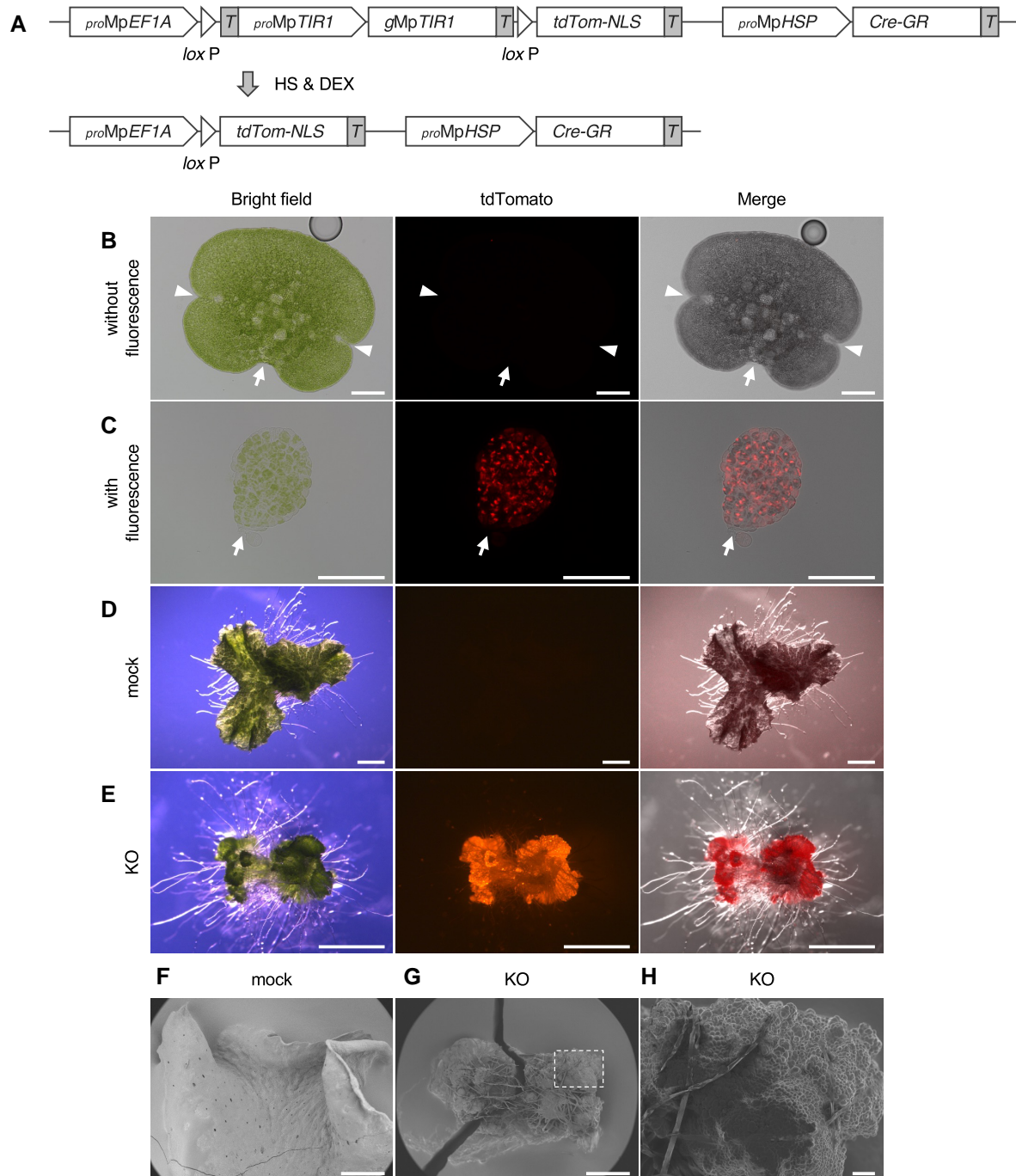


**Figure 5** Physiological functions of MpTIR1 in establishing the plant body axis. A, Scheme of the conditional knockout (CKO) system in *Mptir1-1<sup>CKO > tdTN</sup>* plants. An MpTIR1 genomic sequence for complementation (top) can be excised by recombination between the flanking *loxP* sequences after heat shock and DEX treatment (bottom), causing the KO of MpTIR1. T: NOS terminator. B and C, Defects in gemma development after CKO of MpTIR1. *Mptir1-1<sup>CKO > tdTN</sup>* gemmae were grown for 14 days and subjected to KO induction. After further growth for 8 days, the gemmae on these plants were observed. Representative gemmae that did not (B) or did (C) show tdTomato-fluorescence are shown. D and E, Post-germination defects of gemmae after CKO of MpTIR1. *Mptir1-1<sup>CKO > tdTN</sup>* gemmae were directly subjected to mock-treatment (D) or KO-induction (E) and further grown for 14 days. F–H, Superficial structures of plants after CKO of MpTIR1. *Mptir1-1<sup>CKO > tdTN</sup>* gemmae were directly subjected to mock-treatment (F) or KO-induction (G and H), further cultured for 22 days, and observed by SEM. H, A magnified image of the area within the dotted line in (G). Plants with overall tdTomato fluorescence were manually selected as KO-induced samples. Scale bars = 100  $\mu$ m (B, C, H), 2 mm (D, E), 1 mm (F, G).

(Supplemental Data Set 7), *Mptir1-1<sup>ko</sup>* cells showed significantly lower expression of known transcription factor genes involved in rhizoid and organ differentiation, such as LOTUS

JAPONICUS ROOTHAIRLESS1-LIKE homolog (MpLRL; Breuninger et al., 2016), ROOT HAIR DEFECTIVE SIX-LIKE1 homolog (MpRSL1; Prout et al., 2016), and WIP homolog



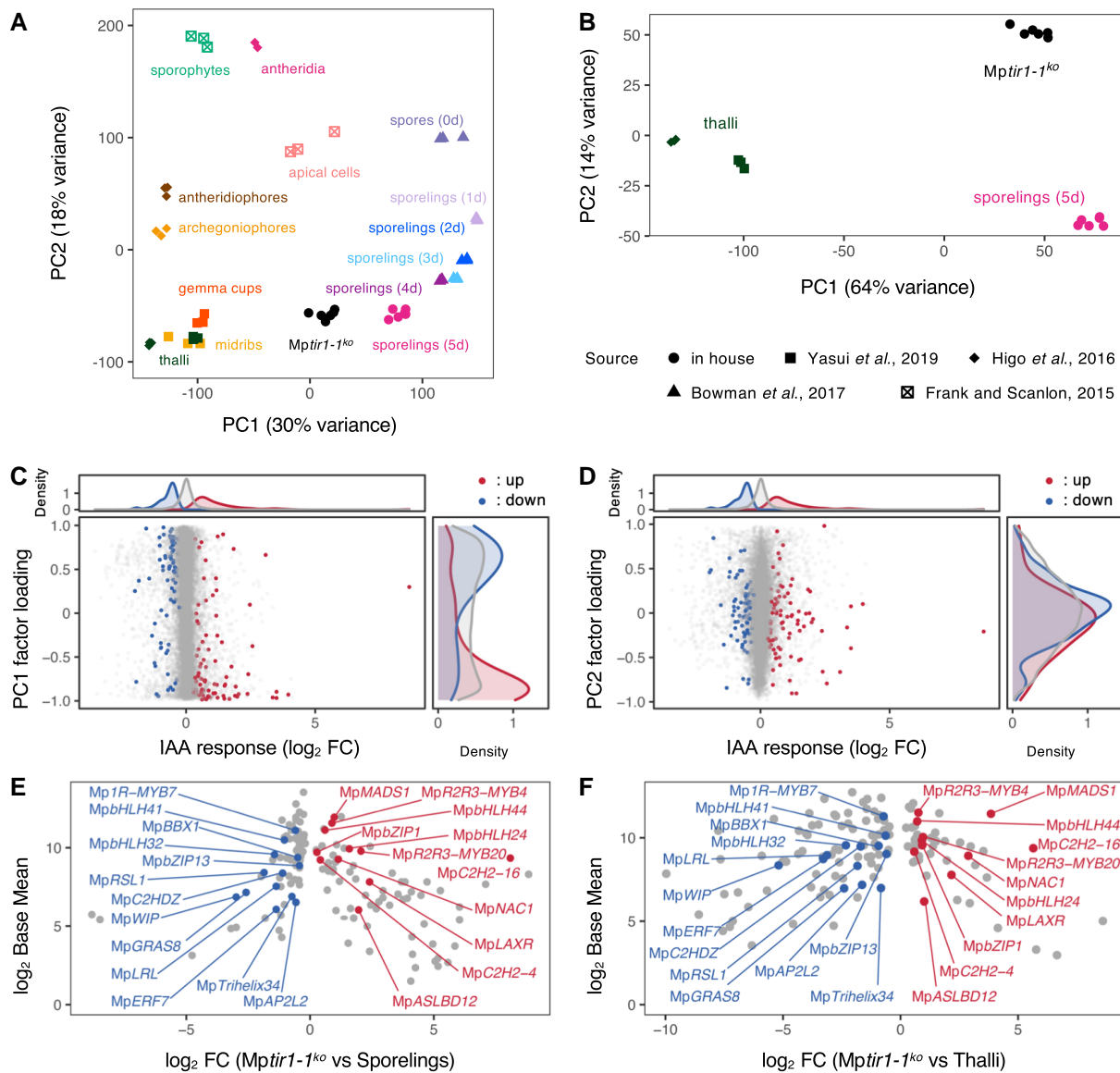


**Figure 6** Characteristics of the *Mptir1-1<sup>ko</sup>* transcriptome. A and B, PCA of transcriptomes obtained from *Mptir1-1<sup>ko</sup>* cells and representative *M. polymorpha* tissues. Expression profiles of all genes were used for calculation. B, Re-calculated PCA with a subset including thalli, 5-day-old sporelings, and *Mptir1-1<sup>ko</sup>* cells. Dots indicate PC1 and PC2 scores of each dataset. Names of tissues or cells are shown near dots of the same color. Dot shapes indicate the sources of RNA-seq data. C and D, Contribution of IAA-responsive genes to factor loading. x-axis of the central panels represents  $\log_2$  FC upon IAA treatment in sporelings. y-axis of the central panels represents the factor loading of PC1 (C) or PC2 (D) of the PCA in (B). Red and blue dots indicate significantly ( $p_{adj} < 0.001$ ) up- and downregulated genes upon IAA treatment, respectively, and gray dots represent IAA-non-responsive genes. Top and right panels represent distribution densities of the colored dots along x- and y-axes, respectively. E and F, Expression profiles of transcription factor genes in *Mptir1-1<sup>ko</sup>* cells. Each dot represents differentially expressed transcription factor genes in *Mptir1-1<sup>ko</sup>* mutants compared with sporelings (E) or thalli (F). Red or blue dots with annotations are genes found in both comparisons. x- and y-axes represent  $\log_2$  FC and  $\log_2$  Base Mean (mean of normalized counts of all samples), respectively.

(*MpWIP*; Jones and Dolan, 2017) compared to sporelings and thalli (Figure 6, E and F). Conversely, *Mptir1-1<sup>ko</sup>* cells highly expressed *LOW-AUXIN RESPONSIVE* (*MpLAXR*), which triggers cellular reprogramming to generate undifferentiated cells (Figure 6, E and F; Ishida et al., 2022). Auxin appears to regulate the *MpTIR1*-dependent expression of these transcription factor genes (Supplemental Figure 12, C–F). Our analyses indicate that *MpTIR1* plays a critical

role in organogenesis by promoting gene expression for differentiation.

## Discussion

### *MpTIR1* is an evolutionarily conserved auxin receptor

In this study, we observed a positive correlation between *MpTIR1* expression levels and auxin responsiveness

(Figure 1; Supplemental Figures 1 and 2, D and E). We observed an auxin-dependent direct interaction of MpTIR1 with DII of MpIAA (Figure 2, A and B), which promoted the degradation of DII-tagged proteins (Figure 2, C and D). *Mptir1-1<sup>ko</sup>* mutants were rescued by AtTIR1 (Figure 1D), which further established the role of MpTIR1 as an auxin receptor. In *M. polymorpha*, MpTIR1 transmits auxin signal by targeting MpIAA for degradation, which allows transcriptional activation as well as competitive repression mediated by the sole class-A and class-B ARFs MpARF1 and MpARF2, respectively (Flores-Sandoval et al., 2015; Kato et al., 2015, 2017, 2020a). Recently, an additional function of AtTIR1 as an adenylate cyclase was reported (Qi et al., 2022). It would be interesting to examine whether MpTIR1 has adenylate cyclase activity and how it affects auxin signaling and plant development in *M. polymorpha*.

In *M. polymorpha*, treatment with auxin, regardless of its type, up- and downregulated similar numbers of genes, implying that TIR1-mediated gene repression is as important as TIR1-mediated gene activation. The downregulated genes included auxin biosynthesis genes such as MpTAA and MpYUC2 (Supplemental Figures 5–7), suggesting their critical role in auxin homeostasis. Considering that YUC genes are also downregulated by auxin treatment in other land plants (Lavy et al., 2016; Takato et al., 2017; Mutte et al., 2018), this feedback regulation appears to be widely conserved. However, whether these responses are directly controlled by auxin signaling or are secondary transcriptional responses remains to be confirmed.

The synthetic auxins NAA and 2,4-D inhibit the growth of *M. polymorpha* much more severely than IAA (Ishizaki et al., 2012). In this study, *M. polymorpha* exhibited a much higher number of DEGs in response to NAA treatment vs. IAA treatment (Figure 3A). However, the amplitude of gene activation or repression by IAA and NAA was comparable with respect to the DEGs regulated by both IAA and NAA (Supplemental Figure 4B). The pull-down assay demonstrated that both IAA and NAA facilitated the interaction between MpTIR1 and MpIAA (Figure 2A). These results suggest that although IAA and NAA both promote MpIAA degradation and enhance transcriptional regulation, we cannot conclude that either of these phytohormones is functionally stronger in terms of MpTIR1-mediated auxin signaling. Nevertheless, NAA still caused growth arrest and transcriptional changes in *Mptir1-1<sup>ko</sup>* cells (Supplemental Figures 2, D and E and 8). One possible explanation is that these processes are mediated by an alternative auxin receptor that prefers NAA to IAA. If so, since AUXIN BINDING PROTEIN 1 is absent in *M. polymorpha* (Bowman et al., 2017; Friml et al., 2022), the hypothetical auxin receptor would be the homolog of S-PHASE KINASE-ASSOCIATED PROTEIN 2, MpSKP2A (Jurado et al., 2010; Bowman et al., 2017), or as-yet-unknown proteins. As alternative scenarios, the non-auxin-specific effects of NAA (Paponov et al., 2019) or differences in the uptake rate by passive diffusion between NAA and IAA (Delbarre et al., 1996) might be reflected in their different effects on *M. polymorpha*.

### MpTIR1-mediated auxin signaling is essential for 3D morphogenesis but not for cell survival

The observations made in this study that KO mutants of MpTIR1 were viable (Figure 4, A–C; Supplemental Figures 9 and 11) are in line with a previous report indicating that *tir1/afb* sextuple mutations did not affect gametophyte viability in *A. thaliana* (Prigge et al., 2020). These results seem to indicate that gametophyte viability is not related to TIR1/AFB-mediated auxin signaling.

In *M. polymorpha*, low auxin levels due to MpTAA KO or overexpression of IAA conjugation enzyme resulted in cell masses in sporelings (Eklund et al., 2015; Flores-Sandoval et al., 2015). In this study, MpTIR1 KO mimicked these phenotypes, suggesting that the cell mass phenotype is largely due to the loss of MpTIR1-mediated auxin signaling. Similarly, blocking auxin signaling via the induction of non-degradable MpIAA (Kato et al., 2015) and recruitment of its co-repressor MpTOPLESS (MpTPL) to MpARFs (Flores-Sandoval et al., 2015) was shown to cause auxin-insensitive cell-mass formation. In these situations, ARF-mediated transcriptional regulation is constitutively repressed regardless of the auxin level, and thus these phenomena are most likely reflected by the cell mass phenotype resulting from MpTIR1 KO (Figures 4 and 5; Supplemental Figures 3 and 11). Strongly overexpressed miRNA-resistant MpARF3 alleles also cause the formation of auxin-insensitive cell masses (Flores-Sandoval et al., 2018). However, it should be noted that there is no direct evidence that MpARF3 functions in the MpTIR1-mediated auxin signaling pathway (Kato et al., 2020a), and therefore, the relationship between the cell mass phenotype and auxin insensitivity is unconfirmed in this case.

Importantly, KO mutants of MpARF1, the sole activator-ARF homolog (Kato et al., 2015), grew as thalli and therefore showed much milder phenotypic effects than *Mptir1* mutants, although they were both insensitive to auxin (Kato et al., 2017). This could be explained by the impaired recruitment of MpIAA to MpARF1 target loci in *Mparf1* mutants, and thus, neither transcriptional activation nor strong repression occurs regardless of auxin levels (Kato et al., 2017, 2018, 2020a). We cannot exclude the possibility that MpARF2 and/or MpARF3 function downstream of MpTIR1. Knockout studies of each MpARF in *Mptir1* mutants could provide clues about why *Mptir1* mutants phenotype *Mparf1* mutants physiologically but not phenotypically.

Auxin signaling is thought to control body axis formation during gemma development, as KO of MpARF1 disrupts patterning during this process (Kato et al., 2017). In the current study, CKO of MpTIR1 in immature gemmae led to the formation of structures without notches (Figure 5, B and C), probably due to impaired axis formation. These activities are reminiscent of AtTIR1/AFBs and other downstream elements that control proper patterning in embryogenesis by regulating division orientation in *A. thaliana* (Yoshida et al., 2014; Prigge et al., 2020). These results support the notion that MpTIR1-mediated auxin signaling is essential for the

establishment of the 3D body plan and organogenesis during early development.

As cell migration is restricted by cell walls, cell supply from stem cells toward the appropriate directions is essential for orderly plant development. The control of cell supply is attributed to the regular division of apical cells in bryophytes (Harrison, 2017; Moody, 2020). In *M. polymorpha*, wedge-shaped apical cells, which produce daughter cells toward the dorsal, ventral, and lateral sides, are established during sporeling and gemma development (Shimamura, 2016). In the cell masses of *Mptir1* mutants, the establishment of properly shaped apical cells and/or control of division planes may be impaired (Figure 4, A and B; Supplemental Figure 11). CKO of *MpTIR1* in gemmalings (where the apical cells are already established) also resulted in cell masses (Figure 5, D and E; Supplemental Figure 3, B and C), suggesting the disruption of apical cell functions in the absence of *MpTIR1*. PCA based on transcriptomes revealed clear separation of *Mptir1-1<sup>ko</sup>* cells and sporelings from thalli (Figure 6B) and a positive correlation of auxin-responsive genes to this separation (Figure 6, C and D; Supplemental Figure 12, A and B). *Mptir1-1<sup>ko</sup>* cells showed lower expression of the differentiation-related transcription factor genes *MpLRL*, *MpRSL1*, and *MpWIP* (Breuninger et al., 2016; Proust et al., 2016; Jones and Dolan, 2017) than sporelings and thalli (Figure 6, E and F). Judging from this, even though swelled cells were observed (Figure 4, F and G), *Mptir1-1<sup>ko</sup>* cells were not assumed to be properly differentiated. A relatively mild knockdown of *MpTAA* and *MpYUC2* results in thalli with impaired organogenesis (Eklund et al., 2015), supporting the notion that the auxin response is required for organ differentiation. *Mptir1-1<sup>ko</sup>* cells showed greater expression of the dedifferentiation-related transcription factor gene *MpLAXR* (Ishida et al., 2022) compared to sporelings and thalli (Figure 6, E and F). Although their molecular functions have not yet been characterized, *MpR2R3-MYB20*, a paralogous gene to *GEMMA CUP-ASSOCIATED MYB1* whose overexpression causes undifferentiated cell clumps (Yasui et al., 2019), and *MpNAC1*, an orthologous gene to *CUP-SHAPED COTYLEDONS*, which act as shoot apical meristem-related boundary genes in angiosperms (Verma et al., 2021), were up-regulated in *Mptir1-1<sup>ko</sup>* cells. In the moss *P. patens*, auxin signaling is thought to be low in undifferentiated tissues but high in differentiating tissues (Thelander et al., 2019), highlighting the conserved roles of auxin in regulating proper differentiation in gametophyte-dominant species. It could be said that the lack of auxin responsiveness of mutants results in the disruption of apical cell functions, which in turn affects organ differentiation, eventually leading to the formation of undifferentiated cell masses in *M. polymorpha*.

In conclusion, *MpTIR1*-mediated auxin signaling contributes to the establishment of the 3D plant body axis by regulating apical stem cell functions, including determining the division plane and cell differentiation. These findings, combined with previous reports of other auxin signaling components in *M. polymorpha*, shed light on organogenesis through

the temporal and spatial regulation of auxin signaling in land plants.

## Materials and methods

### Plant materials and growth conditions

Male accession Takaragaike-1 (Tak-1), female accession Takaragaike-2 (Tak-2), and a female accession of their third backcross generation, BC3-38, were used as wild-type (WT) *Marchantia polymorpha* subsp. *ruderalis*. Tak-1 and BC3-38 were used for phenotypic analysis. Tak-1, BC3-38, and BC4 spores, which were obtained by crossing Tak-1 and BC3-38, were used to generate *MpTIR1*-overexpressing (*proMpEF1A:MpTIR1-3xFLAG*) plants. F<sub>1</sub> spores, which were obtained by crossing Tak-1 and Tak-2, were used to generate *Mptir1-1<sup>ko</sup>* and *Mptir1<sup>ld</sup>* mutants. Male *Mptir1-1<sup>ko</sup>* plants were complemented with the *pMpGWB316\_gMpTIR1\_nonstop* vector (see below) and then crossed with BC3-38 to obtain spores expressing *MpTIR1*-tdTomato under the control of the *MpTIR1* promoter.

*M. polymorpha* was cultured on half-strength Gamborg's B5 medium (Gamborg et al., 1968) containing 1% agar under 50–60 μmol photons per m<sup>2</sup> per s continuous white light at 22°C unless otherwise defined. For crossing, *M. polymorpha* was grown in soil under far-red irradiated conditions to induce gametangiophore formation as described previously (Chiyoda et al., 2008).

### Preparation of plasmid constructs

The oligos used in this study are listed in Supplemental Data Set 8.

#### To generate *proMpEF1A:MpTIR1-3xFLAG* plants

The coding sequence (CDS) of *MpTIR1* without the stop codon was amplified from *pENTR\_MpTIR1* using the primer pair *MpTIR1\_entry/MpTIR1\_nonstop* and cloned into *pENTR/D-TOPO* vector (Thermo Fisher Scientific, Waltham, MA, USA) to generate *pENTR\_MpTIR1\_nonstop*. The *MpTIR1* CDS was then transferred into *pMpGWB110* (Ishizaki et al., 2015) using LR Clonase II (Thermo Fisher Scientific) to generate *pMpGWB110\_MpTIR1*, which was then used for *MpTIR1*-overexpression experiments and pull-down assays.

#### For the pull-down assay

The *MpIAA* or *MpIAA<sup>mutDII</sup>* CDS spanning from the 627th codon to the stop codon was amplified from vectors containing the respective sequences (Kato et al., 2015) using the primer pair *EcoRI-MpIAA\_DII/MpIAA-NotI*. The PCR products and the *pGEX6P-1* vector were digested with *EcoRI* (Takara Bio, Shiga, Japan) and *NotI* (Takara Bio) and then ligated to generate *pGEX6P-1\_MpIAA* and *pGEX6P-1\_MpIAA<sup>mutDII</sup>*. Each of these vectors was introduced into *E. coli* Rosetta2(DE3) strain for the induction of recombinant proteins.

*For homologous recombination of the MpTIR1 locus*

5'- and 3'-homologous arms (3,462 and 3,367 bp, respectively) were amplified from a PAC clone including the MpTIR1 locus (pMM23-241G5; Okada et al., 2000) using the primer pairs MpTIR1\_KO\_F1/MpTIR1\_KO\_R1 and MpTIR1\_KO\_F2/MpTIR1\_KO\_R2, respectively. The resulting 5'- and 3'-homologous arms were cloned into pJHY-Tmp1 (Ishizaki et al., 2013), using an In-Fusion HD cloning kit (Clontech, Mountain View, CA) to generate pJHY-Tmp1\_MpTIR1, which was then used for homologous recombination of the MpTIR1 locus.

*For the complementation cassette for MpTIR1*

A genomic fragment spanning from 5,618-bp upstream of the start codon to 1,081-bp downstream of the stop codon was amplified from pMM23-241G5 (Okada et al., 2000) using the primer pair MpTIR1\_usEntry/MpTIR1\_R15 and cloned into the pENTR/D-TOPO vector (Thermo Fisher Scientific) to generate pENTR\_gMpTIR1. The genomic fragment was then transferred into pMpGWB301 (Ishizaki et al., 2015) using LR Clonase II (Thermo Fisher Scientific) to generate pMpGWB301\_gMpTIR1, which was then used for complementation experiments.

*For the expression of AtTIR1 under the control of the MpTIR1 promoter*

An MpTIR1 promoter sequence spanning from 5,618-bp upstream of the start codon to the start codon was amplified from pMM23-241G5 (Okada et al., 2000) using the primer pair MpTIR1\_usEntry/MpTIR1\_R6 and cloned into the pENTR/D-TOPO vector (Thermo Fisher Scientific) to generate pENTR\_proMpTIR1. An N-terminal 3xFLAG-tagged AtTIR1 CDS was amplified from a vector containing the sequences, pAN19\_TIR1 (a kind gift from Keiko U. Torii and Naoyuki Uchida), using the primer pair Ascl-Flag\_F/AtTIR1\_AscI\_R. pENTR\_proMpTIR1 and the 3xFLAG-AtTIR1 PCR products were digested with Ascl (New England Biolabs, MA, USA) and ligated into pENTR\_proMpTIR1 to generate pENTR\_proMpTIR1:3xFLAG-AtTIR1. The resulting *pro*-MpTIR1:3xFLAG-AtTIR1 fragment was then transferred into pMpGWB301 (Ishizaki et al., 2015) using LR Clonase II (Thermo Fisher Scientific) to generate pMpGWB301\_proMpTIR1:3xFLAG-AtTIR1, which was then used for expression studies of AtTIR1 under the control of the MpTIR1 promoter.

*To express MpTIR1-tdTomato under the control of the MpTIR1 promoter*

A genomic fragment spanning from 5,618-bp upstream of the start codon to before the stop codon was amplified from pENTR\_gMpTIR1 using the primer pair MpTIR1\_usEntry/MpTIR1\_nonstop and cloned into the pENTR/D-TOPO vector (Thermo Fisher Scientific) to generate pENTR\_gMpTIR1\_nonstop. The genomic fragment was then transferred into pMpGWB316 (Ishizaki et al., 2015) using

LR Clonase II (Thermo Fisher Scientific) to generate pMpGWB316\_gMpTIR1\_nonstop, which was then used for expression analysis of functional MpTIR1 under the control of the MpTIR1 promoter.

*To generate MpTIR1-1<sup>CKO > tdTN</sup> plants*

A NOS terminator sequence was amplified from a vector containing the sequence, pMpGWB302 (Ishizaki et al., 2015), using the primer pair NotI-NosT\_F/NotI-NosT\_R. The resulting NOS terminator fragment and pENTR\_gMpTIR1 were digested with NotI (Takara Bio) and then ligated to generate pENTR\_NosT-gMpTIR1. The resulting NosT-gMpTIR1 fragment was then transferred into pMpGWB337tdTN (Sugano et al., 2018) using LR Clonase II (Thermo Fisher Scientific) to generate pMpGWB337tdTN\_NosT:gMpTIR1, which was then used for the MpTIR1 CKO experiments.

*To generate MpTIR1-1<sup>CKO > CitN</sup> plants*

The CDS of MpTIR1 was amplified from RNA of WT plants by reverse transcription PCR using the primer pair MpTIR1\_entry/MpTIR1\_stop and cloned into the pENTR/D-TOPO vector (Thermo Fisher Scientific) to generate pENTR\_MpTIR1. The MpTIR1 fragment was then transferred into pMpGWB337 (Nishihama et al., 2016) using LR Clonase II (Thermo Fisher Scientific) to generate pMpGWB337\_MpTIR1, which was then used for MpTIR1 conditional knockout experiments.

*To generate *pro*MpEF1A:DII-mTurquoise2-NLS/MpTIR1-1<sup>CKO > CitN</sup> plants and *pro*MpEF1A:mutDII-mTurquoise2-NLS/MpTIR1-1<sup>cko > CitN</sup> plants*

The DII and *mutDII* sequences of MpIAA were amplified from vectors containing the respective sequences (see Kato et al., 2015) using the primer pair MpIAA\_dN3/MpIAA DII\_R1 and cloned into the pENTR/D-TOPO vector (Thermo Fisher Scientific) to generate pENTR\_DII and pENTR\_mDII. An *mTurquoise2-NLS* fragment was amplified from a vector containing the sequence, pMpGWB337mT2N, using the phosphorylated primer pairs Aor51HI-mT2\_F/NOST\_head\_Sacl-NLS\_mTurq\_R, digested with Sacl (Takara Bio), and then ligated with Aor51HI- (Takara Bio) and Sacl- (Takara Bio) digested pMpGWB203 (Ishizaki et al., 2015) to generate pMpGWB203\_Gateway:mT2N. The DII- and *mutDII*-fragments were transferred into pMpGWB203\_Gateway:mT2N using LR Clonase II (Thermo Fisher Scientific) to generate pMpGWB203-DII-mT2N and pMpGWB203-*mutDII*-mT2N, respectively. These vectors were then used for degradation assays of DII-tagged protein.

*To delete the MpTIR1 locus using CRISPR/Cas9 genome editing*

Oligos encoding each guide RNA (gRNA) sequence were annealed with their corresponding antisense oligos (see Supplemental Data Set 8). The annealed oligos were ligated with Bsal (New England Biolabs)-digested vectors

with the following combinations: 5'gRNA1 and 5'gRNA3 were ligated with pMpGE\_En\_04; 5'gRNA2 and 5'gRNA4 were ligated with pBC-GE12; 3'gRNA1 and 3'gRNA3 were ligated with pBC-GE23; and 3'gRNA2 and 4'gRNA4 were ligated with pBC-GE34. 5'gRNA1/2-, 5'gRNA3/4-, 3'gRNA1/2-, and 3'gRNA3/4-pairs are active guide RNA-pairs for a nickase version of the CRISPR/Cas9 genome-editing system (Hisanaga et al., 2019; Koide et al., 2020). Four vectors including one of the active 5'gRNA-pairs and one of the active 3'gRNA-pairs were digested by BglI (New England Biolabs) and ligated simultaneously. The resulting gRNA expression cassettes were transferred into pMpGE017 using LR Clonase II (Thermo Fisher Scientific) to generate pMpGE017\_MpTIR1\_5'gRNA1/2\_3'gRNA3/4, pMpGE017\_MpTIR1\_5'gRNA3/4\_3'gRNA1/2, and pMpGE017\_MpTIR1\_5'gRNA3/4\_3'gRNA3/4. These vectors were then used for genome editing of the *MpTIR1* locus. The *Mptir1-2<sup>ld</sup>* mutation was generated using pMpGE017\_MpTIR1\_5'gRNA1/2\_3'gRNA3/4. The *Mptir1-3<sup>ld</sup>* and *Mptir1-4<sup>ld</sup>* mutations were generated using pMpGE017\_MpTIR1\_5'gRNA3/4\_3'gRNA1/2. The *Mptir1-5<sup>ld</sup>* mutation was generated using pMpGE017\_MpTIR1\_5'gRNA3/4\_3'gRNA3/4. pMpGE\_En04, pBC-GE12, pBC-GE23, pBC-GE34, and pMpGE017 were developed by Keisuke Inoue at Kyoto University.

### Plant transformation

Binary vectors were transformed into WT plants as previously described (Ishizaki et al., 2008; Kubota et al., 2013). To transform *Mptir1-1<sup>ko</sup>* mutants, *Mptir1-1<sup>ko</sup>* cell masses were cocultured with *Agrobacterium* GV2260 harboring binary vectors in liquid OM51C medium under continuous white light as described above. After 2 or 3 days of co-cultivation, the *Mptir1-1<sup>ko</sup>* cells were washed with sterilized water and cultured on half-strength Gamborg's B5 medium (Gamborg et al., 1968) containing 1% agar, 100 mg/L cefotaxime, and 0.5  $\mu$ M chlorsulfuron for selection.

### Plant genotyping

For genotyping, fragments of plant tissue were crushed in 100  $\mu$ L of buffer (100 mM Tris-HCl (pH 9.5), 1 M KCl, and 10 mM EDTA), diluted with 400  $\mu$ L of sterilized water, and used as templates for PCR.

*Mptir1-1<sup>ko</sup>* candidate plants were genotyped by PCR using crude DNA extracts and primer pairs A (MpTIR1\_L21/MpTIR1\_R12), B (MpTIR1\_L14/MpEF\_GT\_R1), and C (EnSpm\_L2/MpTIR1\_R13; Supplemental Figure 2A), as described previously (Ishizaki et al., 2013).

*Mptir1<sup>ld</sup>* candidate plants were genotyped by amplifying the *MpTIR1* genomic locus from crude DNA extracts using the primer pair MpTIR1\_L30/MpTIR1\_R21. The resulting DNA fragments were treated with Exonuclease I and Shrimp Alkaline Phosphatase (New England Biolabs), purified with a Fast Gene<sup>TM</sup> Gel/PCR Extraction Kit (NIPPON Genetics Co., Tokyo, Japan), and sequenced with the primers MpTIR1\_L45 or MpTIR1\_R20.

Molecular determination of the sex of the plants was performed by amplifying U (female) and V (male) chromosome markers from crude DNA extract, as described previously (Fujisawa et al., 2001) using the modified primer pairs rhf-73F\_new/rhf-73R\_new and rbm-27F\_new/rbm-27R\_new, respectively.

### CKO analysis

To induce KO of *MpTIR1* in young plants, 1-day-old *Mptir1-1<sup>CKO > CitN</sup>*, *proMpEF1A:DII-mTurquoise2-NLS/Mptir1-1<sup>CKO > CitN</sup>*, and *proMpEF1A:mutDII-mTurquoise2-NLS/Mptir1-1<sup>CKO > CitN</sup>* gemmings were treated with approximately 3  $\mu$ L of 10  $\mu$ M dexamethasone (DEX) solution to enable nuclear localization of glucocorticoid receptor (GR)-fused Cre proteins, dried for several minutes, and incubated at 37°C for 1 h. Each gemmaling was treated once more with the same procedure at 4-h intervals.

To induce KO of *MpTIR1* in gemmae, *Mptir1-1<sup>CKO > tdTN</sup>* gemmae were treated with approximately 3  $\mu$ L of 10  $\mu$ M DEX solution, dried for several minutes, and incubated at 37°C for 1 h. Each gemma was treated once more with the same procedure at 4-h intervals.

To induce KO of *MpTIR1* in immature gemmae, 14-day-old *Mptir1-1<sup>CKO > tdTN</sup>* thalli were vacuum-infiltrated with 5  $\mu$ M DEX solution, dried for approximately 20 min, and incubated at 37°C for 1 h. Each thallus was treated twice with the same procedure at 4- to 5-h intervals. The treated thalli were further cultivated under normal conditions for a few weeks. Gemmae were then taken from gemma cups and used for microscopic analysis.

### Sectioning of plant tissues

To observe cell composition, 10-day-old sporelings and *Mptir1-1<sup>ko</sup>* cell masses grown on half-strength Gamborg's B5 agar medium were pre-fixed in 2.5% (v/v) glutaraldehyde and 2% (w/v) paraformaldehyde in 50 mM phosphate buffer (pH 7.2) at 4°C overnight. The samples were then washed with 50 mM phosphate buffer, and treated with 2% (w/v) OsO<sub>4</sub> solution at room temperature for 2 h, and washed with 8% (w/v) sucrose. The samples were then dehydrated by 25%, 50%, and 80% (v/v) ethanol solutions before being dehydrated in 100% (v/v) ethanol and embedded in the resin Quetol 812 (Nissin EM Co., Kyoto, Japan). The resin-embedded samples were cut into 1  $\mu$ m sections with a diamond knife using Ultracut-UCT (Leica, Wetzlar, Germany). The sections were stained with toluidine blue solution and used for microscopic analysis.

### Microscopic analysis

Thalli, sporelings, and *Mptir1* cell masses were observed using an SZX16 stereo microscope (Olympus, Tokyo, Japan), M205C stereo microscope (Leica, Wetzlar, Germany), Axiophot fluorescence microscope (Zeiss, Oberkochen, Germany), or BZ-X710 fluorescence microscope (Keyence, Osaka, Japan). Plate cultures were photographed using an EOS Kiss X3 digital camera (Canon, Tokyo, Japan). Z-series

images of 2-day-old *proMpEF1A:mutDII-mTurquoise2-NLS/Mptir1-1<sup>CKO > CitN</sup>* plant notches were taken under an FLUOVIEW FV1000 confocal microscope (Olympus). SEM images of *Mptir1* cell masses and *Mptir1-1<sup>CKO > tdTN</sup>* plants were taken under a TM3000 tabletop scanning electron microscope (Hitachi High Technologies, Tokyo, Japan) as described previously (Nishihama et al., 2015).

### Image manipulations

Bright-field (BF) and fluorescence images taken under the M205C stereo microscope were merged using Fiji image analysis software (<http://fiji.sc/>; Schindelin et al., 2012). Z-series confocal images were two-dimensionally projected with max intensity and then merged using Fiji. BF and fluorescence images taken under a BZ-X710 fluorescence microscope were merged using BZ-X Analyzer (Keyence).

### Measurement of plant area

Plant area measurements were performed using Fiji. Bright field images were split into RGB channels using the “Split Channels” function. B-channel images were converted into binary images using the “Auto Threshold” function with the “Default” method. Plant areas were then measured with the “Find Edges” function, followed by the “Analyze Particles” function.

### Quantification of nuclear fluorescence intensities

Images of 2-day-old *proMpEF1A:DII-mTurquoise2-NLS/Mptir1-1<sup>CKO > CitN</sup>* or *proMpEF1A:mutDII-mTurquoise2-NLS/Mptir1-1<sup>CKO > CitN</sup>* plant notches, which were cultured for 1 day after KO induction, were quantified using Fiji by measuring mTurquoise2 fluorescence intensities in the nuclei. Five to six independent plants were observed as biological replicates for each condition. A series of 45 confocal images at 5- $\mu$ m intervals were two-dimensionally projected with sum intensity of the slices. From each image, nucleus and background regions were manually selected as 8- $\mu$ m diameter circles at 25 locations each. The average intensity value of each nucleus region was obtained by subtracting the mean values of background regions from the same image. The data generated were plotted and was analyzed for statistical significance (see “Statistical analysis and graphics” section).

### Pull-down assay

*E. coli* Rosetta2(DE3) cells harboring the GST-MpIAA(627C) or GST-MpIAA<sup>mutDII</sup>(627C) vectors were precultured in 5 mL of LB liquid medium at 37°C overnight. The cultures were then inoculated into 300 mL of fresh LB medium and incubated at 37°C until the OD<sub>600</sub> reached 0.5. Isopropyl  $\beta$ -D-thiogalactopyranoside (IPTG) was added to the culture at a final concentration of 0.1 mM to induce protein expression; the cultures were incubated at 37°C for 5 h. After 5 h, the cells were harvested by centrifugation for 10 min at 4,000 $\times$ g at 4°C, resuspended in ice-cold sonication buffer (PBS and 1 mM dithiothreitol), and subjected to lysis by sonication. The cell lysates were then centrifuged for 30 min at

12,000 $\times$ g at 4°C. The supernatants were purified through Pierce<sup>TM</sup> Disposable Plastic Columns (Thermo Fisher Scientific) containing Glutathione Sepharose 4B (GE Healthcare Life Sciences, MA, USA).

Fourteen-day-old *proMpEF1A:MpTIR1-3xFLAG* plants were harvested and immediately frozen in liquid nitrogen. The frozen samples were homogenized with three-fourth volume per gram of tissue of extraction buffer (150 mM NaCl, 100 mM Tris-HCl pH 7.5, 0.5% Nonidet P-40, 10  $\mu$ M dithiothreitol, 1 mM phenylmethanesulfonyl fluoride, 1  $\mu$ g/mL pepstatin A, and 10  $\mu$ M MG132) and melted on ice. Debris was removed by centrifugation at 16,000 $\times$ g at 4°C for 15 min, after which the supernatant was filtered through a 0.45- $\mu$ m pore syringe filter. The protein concentration of the sample was measured using a Bradford Protein Assay Kit (Bio-Rad Laboratories Inc., CA, USA).

2.5 mg of each protein sample was incubated with 10  $\mu$ L of GST-MpIAA(627C)- or GST-MpIAA(627C)-conjugated Glutathione Sepharose beads and auxin at 4°C for 30 min. After three washes with ice-cold extraction buffer, the beads were mixed with 2x Laemmli sample buffer (100 mM Tris-HCl, pH 6.8, 4% [w/v] SDS, 10% [v/v] 2-mercaptoethanol, and 20% [v/v] glycerol) and boiled at 95°C for 5 min. The samples were separated by SDS-PAGE on a 10% acrylamide gel and transferred onto polyvinylidene fluoride membranes (Bio-Rad Laboratories, Inc.). The membranes were incubated with anti-FLAG (1:5,000; catalog #F3165-2MG, Sigma-Aldrich, MO, USA) or anti-GST antibodies (1:2,000; catalog #04435-84, Nacalai tesque, Kyoto, Japan) for 1 h, washed with PBST (PBS and 0.1% Tween-20), and incubated with anti-mouse IgG antibodies (1:10,000; GE Healthcare) for 1 h. Bands were visualized with ECL Prime reagent (GE Healthcare) on an ImageQuant LAS 4,010 system (GE Healthcare).

### RT-qPCR

For RT-qPCR of *MpTIR1*, 10-day-old Tak-1 and *proMpEF1A:MpTIR1-3xFLAG* plants were harvested and immediately frozen in liquid nitrogen. For RT-qPCR of auxin-responsive genes, F<sub>1</sub> spores and *Mptir1-1<sup>ko</sup>* cell masses were precultured in half-strength Gamborg's B5 liquid medium for 5 days, treated with 10  $\mu$ M NAA or solvent control for 4 h, harvested, and immediately frozen in liquid nitrogen. RNA was extracted from the frozen samples using TRIzol (Thermo Fisher Scientific) as described previously (Kubota et al., 2014). Reverse transcription to cDNA and subsequent quantitative PCR were performed as described previously (Kato et al., 2017). The primer pairs *MpTIR1*-qPCR\_F2/*MpTIR1*-qPCR\_R2, *MpC2HDZ*-qPCR\_F1/*MpC2HDZ*-qPCR\_R1, *MpWIP*-qPCR\_F1/*MpWIP*-qPCR\_R1, and *MpEF*-qPCR\_F/*MpEF*-qPCR\_R were used to quantify *MpTIR1*, *MpC2HDZ*, *MpWIP*, and *MpEF1A* transcripts, respectively (Supplemental Data Set 8). *MpEF1A* was used as an internal control. Relative expression levels were calculated by the Pfaffl method (Pfaffl, 2001).

## RNA-sequencing

F<sub>1</sub> spores and *Mptir1-1<sup>ko</sup>* cell masses were precultured in half-strength Gamborg's B5 liquid medium for 5 days and treated with 10 μM IAA or solvent control for 4 h. The plants were harvested and immediately frozen in liquid nitrogen. Three different populations were prepared as biological replicates for each condition. RNA extraction from frozen samples was performed using an RNeasy Plant Mini Kit (QIAGEN, Venlo, the Netherlands). RNA Libraries were prepared using a NEBNext Ultra II Directional RNA Library Prep Kit for Illumina (New England Biolabs) and sequenced as single end reads using the NextSeq500 platform (Illumina, CA, USA). Total RNA was extracted from F<sub>1</sub> spores and *Mptir1-1<sup>ko</sup>* cell masses treated with 10 μM NAA or solvent control in the same manner. Library preparation and subsequent paired-end RNA-sequencing were performed by Macrogen Japan (Tokyo, Japan) using the NovaSeq6000 platform (Illumina).

## Analysis of RNA-seq data

For quality control, raw read data were pre-filtered using fastp (version 0.20.1; [Chen et al., 2018](#)) with default settings for SE- and PE-sequence data, respectively. The filtered reads were then mapped onto the *M. polymorpha* genome (v5.1r1 + U-chromosomal genes of v3.1) using STAR (version 2.6.1c; [Dobin et al., 2013](#)) with default settings for SE- and PE-sequence data, respectively. The following analyses were performed in R (version 4.0.0; [R Core Team, 2020](#)). Reads mapped onto exons were counted using the “featureCounts” function of the Rsubread package (version 2.2.2; [Liao et al., 2019](#)). Pairwise comparisons were performed by Wald test using the DESeq2 package (version 1.28.1; [Love et al., 2014](#)). In the pairwise comparisons between *Mptir1-1<sup>ko</sup>* cells and WT tissues, U chromosomal genes were excluded. All four combinations of comparisons between *Mptir1-1<sup>ko</sup>* cells (mock samples for IAA or those for NAA) and public thalli data (9-day-old thalli from [Higo et al., 2016](#) or 7-day-old thalli from [Yasui et al., 2019](#)) were performed. The shared DEGs among all comparisons were chosen; since all data sets were derived from different experiments, batch effects were not taken into consideration. GO term enrichment and subsequent selection of representative terms were performed with the pipeline described in [Ishida et al. \(2022\)](#). PCA was performed using the “prcomp” function of the stats package (version 4.0.0; [R Core Team, 2020](#)) with log<sub>2</sub> transformed read counts of all genes. Factor loadings were calculated as  $\sqrt{l} \times h_i u_i$ , where  $l$ ,  $h_i$ , and  $u_i$  represent the eigenvalues of the covariance, the eigenvectors of each gene, and the square root of variance of each gene, respectively.

## Statistical analysis and graphics

Statistical tests were performed using R (version 4.0.0; [R Core Team, 2020](#)). The stats package (version 4.0.0; [R Core Team, 2020](#)) was used for Welch's t-test ([Figure 1A](#)) and Pearson's

correlation test ([Supplemental Figure 4B](#)). The NSM3 package (version 1.15; [Schneider et al., 2020](#)) was used for Steel–Dwass test ([Figure 1C](#); [Supplemental Figure 1, B and D](#)). The lawstat package (version 3.4; [Gastwirth et al., 2020](#)) was used for Brunner–Munzel test ([Figure 2D](#)). The mult-comp package (version 1.4.13; [Hothorn et al., 2008](#)) was used for ANOVA and subsequent Tukey–Kramer test ([Figure 3B](#)) and Dunnett test ([Supplemental Figure 2E](#)). The DESeq2 package (version 1.28.1; [Love et al., 2014](#)) was used for Wald test ([Supplemental Data Sets 1, 2, and 6](#)). Graphs were drawn by R using the ggplot2 package (version 3.3.1; [Wickham, 2016](#)), the ggsignif package (version 0.6.0; [Ahlmann-Eltze, 2019](#)), and the UpSetR package (version 1.4.0; [Conway et al., 2017](#); [Gehlenborg, 2019](#)). See [Supplemental Data Set 9](#) for summary of statistical analyses.

## Accession numbers

Sequence data from this article can be found in the GenBank libraries (<http://www.ncbi.nlm.nih.gov>) or the MarpolBase (<https://marchantia.info>) under the following accession numbers: *AtTIR1* (AT3G62980); *MpTIR1* (Mp6g02750/Mapoly0035s0062); *MpIAA* (Mp6g05000/Mapoly0034s0017); *MpARF1* (Mp1g12750/Mapoly0019s0045); *MpARF2* (Mp4g11820/Mapoly0011s0167); *MpARF3* (Mp1g07070/Mapoly0043s0098); *MpNCARF* (Mp2g02890/Mapoly0075s0050); *MpTPL* (Mp7g17410/Mapoly0051s0078); *MpTAA* (Mp5g14320/Mapoly0032s0124); *MpYUC2* (Mp8g08780/Mapoly0063s0040); *MpC2HDZ* (Mp2g24200/Mapoly0069s0069); *MpLRL* (Mpzg01410/Mapoly0502s0001); *MpRSL1* (Mp3g17930/Mapoly0039s0003); *MpWIP* (Mp1g09500/Mapoly0096s0050); *MpR2R3-MYB21* (Mp3g05910/Mapoly1089s0002); *MpLAXR* (Mp5g06970/Mapoly0136s0025); *MpR2R3-MYB20* (Mp4g21790/Mapoly0874s0001); *MpNAC1* (Mp2g07720/Mapoly0015s0058); *MpSKP2A* (Mp8g10660). Other *M. polymorpha* genes used in RNA-seq analysis are listed in [Supplemental Data Set 7](#).

Transcriptome data obtained in this study were deposited in the DNA Data Bank of Japan Sequence Read Archive (<https://www.ddbj.nig.ac.jp/dra>) under project number DRA013690. Other public transcriptome data obtained from the Sequence Read Archive (<https://www.ncbi.nlm.nih.gov/sra>) are listed in [Supplemental Data Set 10](#).

## Supplemental data

The following materials are available in the online version of this article.

**Supplemental Figure S1.** Genetic evidence that *MpTIR1* is involved in the auxin response.

**Supplemental Figure S2.** Genotyping and auxin responses of *Mptir1-1<sup>ko</sup>* mutants.

**Supplemental Figure S3.** Verification of induced *MpTIR1* KO.

**Supplemental Figure S4.** Significant overlap between IAA- and NAA-responsive genes.

**Supplemental Figure S5.** Responses of IAA-responsive genes to NAA and 2,4-D.

**Supplemental Figure S6.** Responses of NAA-responsive genes to IAA and 2,4-D.

**Supplemental Figure S7.** Responses of 2,4-D-responsive genes to IAA and NAA.

**Supplemental Figure S8.** GO terms enriched in genes that responded to NAA in an *MpTIR1*-independent manner.

**Supplemental Figure S9.** Growth of *Mptir1-1<sup>ko</sup>* mutants.

**Supplemental Figure S10.** Generation and genotyping of *MpTIR1*-locus deletion mutants.

**Supplemental Figure S11.** Reproducibility of *Mptir1* defects in *Mptir1<sup>ld</sup>* mutants.

**Supplemental Figure S12.** Contribution of auxin-responsive genes to the transcriptional properties of *Mptir1-1<sup>ko</sup>* cells.

**Supplemental Figure S13.** Transcriptional changes of genes related to auxin biosynthesis and signaling in spores, sporelings, and thalli.

**Supplemental Figure S14.** *MpTIR1* is expressed before the establishment of the 3D body axes.

**Supplemental Data Set 1.** Pairwise comparisons between auxin- and mock-treated samples in WT or *Mptir1-1<sup>ko</sup>* cells.

**Supplemental Data Set 2.** Pairwise comparisons between 2,4-D- and mock-treated WT thalli.

**Supplemental Data Set 3.** Genes that responded to NAA in *Mptir1-1<sup>ko</sup>* cells.

**Supplemental Data Set 4.** GO terms enriched in genes up-regulated by NAA-treatment in *Mptir1-1<sup>ko</sup>* cells.

**Supplemental Data Set 5.** GO terms enriched in genes downregulated by NAA-treatment in *Mptir1-1<sup>ko</sup>* cells.

**Supplemental Data Set 6.** Pairwise comparisons between *Mptir1-1<sup>ko</sup>* cells and WT samples.

**Supplemental Data Set 7.** IDs and names of auxin biosynthesis genes, auxin signaling genes, and transcription factors (TFs) in *M. polymorpha*.

**Supplemental Data Set 8.** Oligos used in this study.

**Supplemental Data Set 9.** Summary of statistical analyses

**Supplemental Data Set 10.** Public RNA-seq data used in this study.

## Acknowledgments

We thank Keiko U Torii and Naoyuki Uchida for kindly providing the vector, pAN19\_TIR1. We thank Keisuke Inoue for kindly providing the vectors, pMpGE\_En04, pBC-GE12, pBC-GE23, pBC-GE34, and pMpGE017. We thank Takefumi Kondo and Yukari Sando for sequencing RNA. We thank Editage (www.editage.com) for English language editing.

## Funding

This work was supported by Grants-in-Aid for Scientific Research (KAKENHI) from the Ministry of Education, Culture, Sports, Science and Technology (MEXT) / Japan Society for the Promotion of Science (JSPS) (grant numbers: JP18J12698 and 21K20649 to H.S., 12J07037, 19K23751, and 21K15125 to H.K., JP16K07398 and JP20H04884 to R.N., and

25113009, JP17H07424, and JP19H05675 to T.K.) and SPIRITS 2017 of Kyoto University to R.N.

*Conflict of interest statement.* The authors declare no competing interests.

## References

- R Core Team (2020) R: A Language and Environment for Statistical Computing. R Foundation for Statistical Computing, Vienna, Austria
- Ahlmann-Eltze C (2019). ggsignif: Significance Brackets for 'ggplot2'. R package version 0.6.0. <https://CRAN.R-project.org/package=ggsignif> (accessed: 30 May 2020)
- Althoff F, Kopischke S, Zobell O, Ide K, Ishizaki K, Kohchi T, Zachgo S (2014) Comparison of the *MpEF1α* and *CaMV35* promoters for application in *Marchantia polymorpha* overexpression studies. *Transgenic Res* 23(2): 235–244
- Bowman JL, Briginshaw LN, Fisher TJ, Flores-Sandoval E (2019) Something ancient and something neofunctionalized—evolution of land plant hormone signaling pathways. *Curr Opin Plant Biol* 47: 64–72
- Bowman JL, Kohchi T, Yamato KT, Jenkins J, Shu S, Ishizaki K, Yamaoka S, Nishihama R, Nakamura Y, Berger F, et al. (2017) Insights into land plant evolution garnered from the *Marchantia polymorpha* genome. *Cell* 171(2): 287–304.e15
- Breuninger H, Thamm A, Streubel S, Sakayama H, Nishiyama T, Dolan L (2016) Diversification of a transcription factor family led to the evolution of antagonistically acting genetic regulators of root hair growth. *Curr Biol* 26(12): 1622–1628
- Chen S, Zhou Y, Chen Y, Gu J (2018) Fastp: an ultra-fast all-in-one FASTQ preprocessor. *Bioinformatics* 34(17): i884–i890
- Chiyoda S, Ishizaki K, Kataoka H, Yamato KT, Kohchi T (2008) Direct transformation of the liverwort *Marchantia polymorpha* L. By particle bombardment using immature thalli developing from spores. *Plant Cell Rep* 27(9): 1467–1473
- Conway JR, Lex A, Gehlenborg N (2017) Upsetr: an R package for the visualization of intersecting sets and their properties. *Bioinformatics* 33(18): 2938–2940
- Delbarre A, Muller P, Imhoff V, Guern J (1996) Comparison of mechanisms controlling uptake and accumulation of 2,4-dichlorophenoxy acetic acid, naphthalene-1-acetic acid, and indole-3-acetic acid in suspension-cultured tobacco cells. *Planta* 198(4): 532–541
- Delwiche CF, Cooper ED (2015) The evolutionary origin of a terrestrial flora. *Curr Biol* 25(19): R899–R910
- Dharmasiri N, Dharmasiri S, Estelle M (2005) The F-box protein TIR1 is an auxin receptor. *Nature* 435(7041): 441–445
- Dobin A, Davis CA, Schlesinger F, Drenkow J, Zaleski C, Jha S, Batut P, Chaisson M, Gingeras TR (2013) STAR: ultrafast universal RNA-seq aligner. *Bioinformatics* 29(1): 15–21
- Eklund DM, Ishizaki K, Flores-Sandoval E, Kikuchi S, Takebayashi Y, Tsukamoto S, Hirakawa Y, Nonomura M, Kato H, Kouno M, et al. (2015) Auxin produced by the indole-3-pyruvic acid pathway regulates development and gemmae dormancy in the liverwort *Marchantia polymorpha*. *Plant Cell* 27(6): 1650–1669
- Flores-Sandoval E, Eklund DM, Bowman JL (2015) A simple auxin transcriptional response system regulates multiple morphogenetic processes in the liverwort *Marchantia polymorpha*. *PLoS Genet* 11(5): e1005207
- Flores-Sandoval E, Eklund DM, Hong S-F, Alvarez JP, Fisher TJ, Lampugnani ER, Golz JF, Vázquez-Lobo A, Dierschke T, Lin S-S, et al. (2018) Class C ARFs evolved before the origin of land plants and antagonize differentiation and developmental transitions in *Marchantia polymorpha*. *New Phytol* 218(4): 1612–1630



- Frank MH, Scanlon MJ (2015) Transcriptomic evidence for the evolution of shoot meristem function in sporophyte-dominant land plants through concerted selection of ancestral gametophytic and sporophytic genetic programs. *Mol Biol Evol* **32**(2): 355–367
- Friml J, Gallei M, Gelová Z, Johnson A, Mazur E, Monzer A, Rodriguez L, Roosjen M, Verstraeten I, Živanović BD, et al. (2022) ABP1-TMK Auxin perception mediates ultrafast global phosphorylation and auxin canalization. *Nature* **609**(7927): 575–581
- Fujisawa M, Hayashi K, Nishio T, Bando T, Okada S, Yamato KT, Fukuzawa H, Ohyania K (2001) Isolation of X and Y chromosome-specific DNA markers from a liverwort, *Marchantia polymorpha*, by representational difference analysis. *Genetics* **159**(3): 981–985
- Gaal DJ, Dufresne SJ, Maravolo NC (1982) Transport of <sup>14</sup>C-indoleacetic acid in the hepatic *Marchantia polymorpha*. *Bryologist* **85**(4): 410–418
- Galvan-Ampudia CS, Cerutti G, Legrand J, Brunoud G, Martin-Arevalillo R, Azais R, Bayle V, Moussu S, Wenzl C, Jaillais Y, et al. (2020) Temporal integration of auxin information for the regulation of patterning. *eLife* **9**: e55832
- Gamborg OL, Miller RA, Ojima K (1968) Nutrient requirements of suspension cultures of soybean root cells. *Exp Cell Res* **50**(1): 151–158
- Gastwirth JL, Gel YR, Hui WLW, Lyubchich V, Miao W, Noguchi K (2020). lawstat: Tools for Biostatistics, Public Policy, and Law. R package version 3.4. <https://CRAN.R-project.org/package=lawstat> (accessed: 30 May 2020)
- Gehlenborg N (2019). UpSetR: A More Scalable Alternative to Venn and Euler Diagrams for Visualizing Intersecting Sets. R package version 1.4.0. <https://CRAN.R-project.org/package=UpSetR> (accessed: 30 May 2020)
- Gray WM, del Pozo JC, Walker L, Hobbie L, Risseuw E, Banks T, Crosby WL, Yang M, Ma H, Estelle M (1999) Identification of an SCF ubiquitin-ligase complex required for auxin response in *Arabidopsis thaliana*. *Genes Dev* **13**(13): 1678–1691
- Gray WM, Kepinski S, Rouse D, Leyser O, Estelle M (2001) Auxin regulates SCF<sup>TIR1</sup>-dependent degradation of AUX/IAA proteins. *Nature* **414**(6861): 271–276
- Guan C, Jiao Y (2020) Interplay between the shoot apical meristem and lateral organs. *Abiotech* **1**(3): 178–184
- Harrison CJ (2017) Development and genetics in the evolution of land plant body plans. *Philos Trans R Soc Lond B Biol Sci* **372**(1713): 20150490
- Herud-Sikimić O, Stiel AC, Kolb M, Shanmugaratnam S, Berendzen KW, Feldhaus C, Höcker B, Jürgens G (2021) A biosensor for the direct visualization of auxin. *Nature* **592**(7856): 768–772
- Higo A, Niwa M, Yamato KT, Yamada L, Sawada H, Sakamoto T, Kurata T, Shirakawa M, Endo M, Shigenobu S, et al. (2016) Transcriptional framework of male gametogenesis in the liverwort *Marchantia polymorpha* L. *Plant Cell Physiol* **57**(2): 325–338
- Hisanaga T, Okahashi K, Yamaoka S, Kajiwara T, Nishihama R, Shimamura M, Yamato KT, Bowman JL, Kohchi T, Nakajima K (2019) A cis-acting bidirectional transcription switch controls sexual dimorphism in the liverwort. *EMBO J* **38**(6): e100240
- Hothorn T, Bretz F, Westfall P (2008) Simultaneous inference in general parametric models. *Biometrical J* **50**(3): 346–363
- Ishida S, Suzuki H, Iwaki A, Kawamura S, Yamaoka S, Kojima M, Takebayashi Y, Yamaguchi K, Shigenobu S, Sakakibara H, et al. (2022) Diminished auxin signaling triggers cellular reprogramming by inducing a regeneration factor in the liverwort *Marchantia polymorpha*. *Plant Cell Physiol* **63**(3): 384–400
- Ishizaki K, Chiyoda S, Yamato KT, Kohchi T (2008) *Agrobacterium*-mediated transformation of the haploid liverwort *Marchantia polymorpha* L., an emerging model for plant biology. *Plant Cell Physiol* **49**(7): 1084–1091
- Ishizaki K, Johzuka-Hisatomi Y, Ishida S, Iida S, Kohchi T (2013) Homologous recombination-mediated gene targeting in the liverwort *Marchantia polymorpha* L. *Sci Rep* **3**(1): 1532
- Ishizaki K, Nishihama R, Ueda M, Inoue K, Ishida S, Nishimura Y, Shikanai T, Kohchi T (2015) Development of gateway binary vector series with four different selection markers for the liverwort *Marchantia polymorpha*. *PLoS One* **10**(9): e0138876
- Ishizaki K, Nonomura M, Kato H, Yamato KT, Kohchi T (2012) Visualization of auxin-mediated transcriptional activation using a common auxin-responsive reporter system in the liverwort *Marchantia polymorpha*. *J Plant Res* **125**(5): 643–651
- Jones VAS, Dolan L (2017) MpWIP regulates air pore complex development in the liverwort *Marchantia polymorpha*. *Development* **144**(8): 1472–1476
- Jurado S, Abraham Z, Manzano C, López-Torrejón G, Pacios LF, Del Pozo JC (2010) The *Arabidopsis* cell cycle F-box protein SKP2A binds to auxin. *Plant Cell* **22**(12): 3891–3904
- Kato H, Ishizaki K, Kouno M, Shirakawa M, Bowman JL, Nishihama R, Kohchi T (2015) Auxin-mediated transcriptional system with a minimal set of components is critical for morphogenesis through the life cycle in *Marchantia polymorpha*. *PLoS Genet* **11**(5): e1005084
- Kato H, Kouno M, Takeda M, Suzuki H, Ishizaki K, Nishihama R, Kohchi T (2017) The roles of the sole activator-type auxin response factor in pattern formation of *Marchantia polymorpha*. *Plant Cell Physiol* **58**(10): 1642–1651
- Kato H, Mutte SK, Suzuki H, Crespo I, Das S, Radoeva T, Fontana M, Yoshitake Y, Hainiwa E, van den Berg W, et al. (2020a) Design principles of a minimal auxin response system. *Nat Plants* **6**(5): 473–482
- Kato H, Nishihama R, Weijers D, Kohchi T (2018) Evolution of nuclear auxin signaling: lessons from genetic studies with basal land plants. *J Exp Bot* **69**(2): 291–301
- Kato H, Yasui Y, Ishizaki K (2020b) Gemma cup and gemma development in *Marchantia polymorpha*. *New Phytol* **228**(2): 459–465
- Kepinski S, Leyser O (2005) The *Arabidopsis* F-box protein TIR1 is an auxin receptor. *Nature* **435**(7041): 446–451
- Kim J, Harter K, Theologis A (1997) Protein–protein interactions among the Aux/IAA proteins. *Proc Natl Acad Sci U S A* **94**(22): 11786–11791
- Kohchi T, Yamato KT, Ishizaki K, Yamaoka S, Nishihama R (2021) Development and molecular genetics of *Marchantia polymorpha*. *Annu Rev Plant Biol* **72**(1): 1–26
- Koide E, Suetsugu N, Iwano M, Gotoh E, Nomura Y, Stolze SC, Nakagami H, Kohchi T, Nishihama R (2020) Regulation of photosynthetic carbohydrate metabolism by a raf-like kinase in the liverwort *Marchantia polymorpha*. *Plant Cell Physiol* **61**(3): 631–643
- Kubota A, Ishizaki K, Hosaka M, Kohchi T (2013) Efficient *Agrobacterium*-mediated transformation of the liverwort *Marchantia polymorpha* using regenerating thalli. *Biosci Biotechnol Biochem* **77**(1): 167–172
- Kubota A, Kita S, Ishizaki K, Nishihama R, Yamato KT, Kohchi T (2014) Co-option of a photoperiodic growth-phase transition system during land plant evolution. *Nat Commun* **5**(1): 3668
- Lavy M, Prigge MJ, Tao S, Shain S, Kuo A, Kirchsteiger K, Estelle M (2016) Constitutive auxin response in *Physcomitrella* reveals complex interactions between Aux/IAA and ARF proteins. *eLife* **5**: e13325
- Liao C-Y, Smet W, Brunoud G, Yoshida S, Vernoux T, Weijers D (2015) Reporters for sensitive and quantitative measurement of auxin response. *Nat Methods* **12**(3): 207–210
- Liao Y, Smyth GK, Shi W (2019) The R package Rsubread is easier, faster, cheaper and better for alignment and quantification of RNA sequencing reads. *Nucleic Acids Res* **47**(8): e47
- Love MI, Huber W, Anders S (2014) Moderated estimation of fold change and dispersion for RNA-seq data with DESeq 2. *Genome Biol* **15**(12): 550
- Moody LA (2020) Three-dimensional growth: a developmental innovation that facilitated plant terrestrialization. *J Plant Res* **133**(3): 283–290
- Mutte SK, Kato H, Rothfels C, Melkonian M, Wong GK-S, Weijers D (2018) Origin and evolution of the nuclear auxin response system. *eLife* **7**: e33399

- Nishihama R, Ishida S, Urawa H, Kamei Y, Kohchi T** (2016) Conditional gene expression/deletion systems for *Marchantia polymorpha* using its own heat-shock promoter and Cre/loxP-mediated site-specific recombination. *Plant Cell Physiol* **57**(2): 271–280
- Nishihama R, Ishizaki K, Hosaka M, Matsuda Y, Kubota A, Kohchi T** (2015) Phytochrome-mediated regulation of cell division and growth during regeneration and sporeling development in the liverwort *Marchantia polymorpha*. *J Plant Res* **128**(3): 407–421
- Okada S, Fujisawa M, Sone T, Nakayama S, Nishiyama R, Takenaka M, Yamaoka S, Sakaida M, Kono K, Takahama M, et al.** (2000) Construction of male and female PAC genomic libraries suitable for identification of Y-chromosome-specific clones from the liverwort, *Marchantia polymorpha*. *Plant J* **24**(3): 421–428
- Paponov IA, Friz T, Budnyk V, Teale W, Wüst F, Paponov M, Al-Babili S, Palme K** (2019) Natural auxin does not inhibit Brefeldin A induced PIN1 and PIN2 internalization in root cells. *Front Plant Sci* **10**: 1–7
- Pfaffl MW** (2001) A new mathematical model for relative quantification in real-time RT-PCR. *Nucleic Acids Res* **29**(9): e45
- Prigge MJ, Lavy M, Ashton NW, Estelle M** (2010) *Physcomitrella patens* auxin-resistant mutants affect conserved elements of an auxin-signaling pathway. *Curr Biol* **20**(21): 1907–1912
- Prigge MJ, Platre M, Kadakia N, Zhang Y, Greenham K, Szutu W, Pandey BK, Bhosale RA, Bennett MJ, Busch W, et al.** (2020) Genetic analysis of the Arabidopsis TIR1/AFB auxin receptors reveals both overlapping and specialized functions. *eLife* **9**: e54740
- Proust H, Honkanen S, Jones VAS, Morieri G, Prescott H, Kelly S, Ishizaki K, Kohchi T, Dolan L** (2016) RSL Class I genes controlled the development of epidermal structures in the common ancestor of land plants. *Curr Biol* **26**(1): 93–99
- Qi L, Kwiatkowski M, Chen H, Hoermayer L, Sinclair S, Zou M, del Genio CI, Kubeš MF, Napier R, Jaworski K, et al.** (2022) Adenylate cyclase activity of TIR1/AFB auxin receptors in plants. *Nature* **611**(7934): 133–138
- Resning SA, Goffinet B, Meyberg R, Wu SZ, Bezanilla M** (2020) The moss *physcomitrium* (*Physcomitrella*) *patens*: a model organism for non-seed plants. *Plant Cell* **32**(5): 1361–1376
- Schindelin J, Arganda-Carreras I, Frise E, Kaynig V, Longair M, Pietzsch T, Preibisch S, Rueden C, Saalfeld S, Schmid B, et al.** (2012) Fiji: an open-source platform for biological-image analysis. *Nat Methods* **9**(7): 676–682
- Schneider G, Chicken E, Becvarik R** (2020). NSM3: Functions and Datasets to Accompany Hollander, Wolfe, and Chicken-Nonparametric Statistical Methods, Third Edition. R package version 1.15. <https://CRAN.R-project.org/package=NSM3> (accessed: 22 February 2021)
- Shimamura M** (2016) *Marchantia polymorpha*; taxonomy, phylogeny, and morphology of a model system. *Plant Cell Physiol* **57**(2): 230–256
- Solly JE, Cunniffe NJ, Harrison CJ** (2017) Regional growth rate differences specified by apical notch activities regulate liverwort thallus shape. *Curr Biol* **27**(1): 16–26
- Su SH, Gibbs NM, Jancewicz AL, Masson PH** (2017) Molecular mechanisms of root gravitropism. *Curr Biol* **27**(17): R964–R972
- Sugano SS, Nishihama R, Shirakawa M, Takagi J, Matsuda Y, Ishida S, Shimada T, Hara-Nishimura I, Osakabe K, Kohchi T** (2018) Efficient CRISPR/Cas9-based genome editing and its application to conditional genetic analysis in *Marchantia polymorpha*. *PLoS One* **13**(10): 1–22
- Suzuki H, Harrison CJ, Shimamura M, Kohchi T, Nishihama R** (2020) Positional cues regulate dorsal organ formation in the liverwort *Marchantia polymorpha*. *J Plant Res* **133**(3): 311–321
- Szemenyei H, Hannon M, Long JA** (2008) TOPLESS Mediates auxin-dependent transcriptional repression during *Arabidopsis* embryogenesis. *Science* **319**(5868): 1384–1386
- Takato S, Kakei Y, Mitsui M, Ishida Y, Suzuki M, Yamazaki C, Hayashi KI, Ishii T, Nakamura A, Soeno K, et al.** (2017) Auxin signaling through SCF<sup>TIR1/AFBs</sup> mediates feedback regulation of IAA biosynthesis. *Biosci Biotechnol Biochem* **81**(7): 1320–1326
- Tan X, Calderon-Villalobos LIA, Sharon M, Zheng C, Robinson CV, Estelle M, Zheng N** (2007) Mechanism of auxin perception by the TIR1 ubiquitin ligase. *Nature* **446**(7136): 640–645
- Thelander M, Landberg K, Sundberg E** (2019) Minimal auxin sensing levels in vegetative moss stem cells revealed by a ratiometric reporter. *New Phytol* **224**(2): 775–788
- Tiwari SB, Hagen G, Guilfoyle T** (2003) The roles of auxin response factor domains in auxin-responsive transcription. *Plant Cell* **15**(2): 533–543
- Ulmasov T, Hagen G, Guilfoyle TJ** (1997) ARF1, a transcription factor that binds to auxin response elements. *Science* **276**(5320): 1865–1868
- Ulmasov T, Hagen G, Guilfoyle TJ** (1999) Dimerization and DNA binding of auxin response factors. *Plant J* **19**(3): 309–319
- Verma S, Attuluri VPS, Robert HS** (2021) An essential function for auxin in embryo development. *Cold Spring Harb Perspect Biol* **13**(4): a039966
- Wickham H** (2016) ggplot2: Elegant Graphics for Data Analysis. Springer-Verlag, New York
- Yasui Y, Tsukamoto S, Sugaya T, Nishihama R, Wang Q, Kato H, Yamato KT, Fukaki H, Mimura T, Kubo H, et al.** (2019) GEMMA CUP-ASSOCIATED MYB1, an ortholog of axillary meristem regulators, is essential in vegetative reproduction in *Marchantia polymorpha*. *Curr Biol* **29**(23): 3987–3995.e5
- Yoshida S, BarbierdeReuille P, Lane B, Bassel GW, Prusinkiewicz P, Smith RS, Weijers D** (2014) Genetic control of plant development by overriding a geometric division rule. *Dev Cell* **29**(1): 75–87